LBL-3175
c.1

ELECTRODEPOSITION AROUND PROTRUDING SURFACE IMPERFECTIONS IN TURBULENT FLOW

Eric John Carlson
(M.S. thesis)

January, 1975

Prepared for the U. S. Atomic Energy Commission
under Contract W-7405-ENG-48

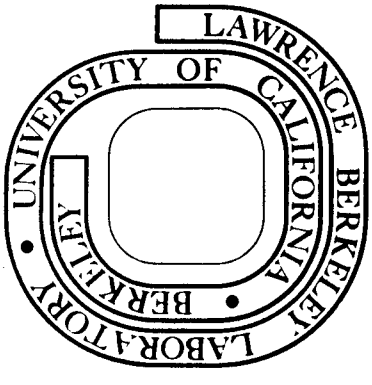

LBL-3175
c.1

DISCLAIMER

I. INTRODUCTION

In electrochemical processes such as electroforming and "high speed" plating one would like to operate at the highest possible rates which still yield a satisfactory product. To achieve the surface finishes required, it has been necessary to employ addition agents and to operate at levels far below the limiting current. The selection of the optimal operating conditions and electrolyte compositions in present day electroplating has developed into a high art akin to alchemy with little exchange of information among the interested parties. While proceeding in this search for the "ultimate" plating bath, the importance of mass transfer and hydrodynamics have often been neglected. These topics become dominant factors in the plating process as the rate approaches the maximum attainable level, the limiting current. Surface defects and blemishes in the deposit resulting from particulate matter, bubbles, or imperfections in the original substrate increase as the stirring level rises and the limiting current is approached. The published literature contains no reports of the micro-hydrodynamics and accompanying morphological changes associated with these isolated roughness elements in either laminar or turbulent flow. The overall mass transfer coefficients reported for homogeneously roughened surfaces do not provide any insight into the phenomena occurring on the scale of the roughness.[1,2]

This study was initiated to obtain a comprehensive view of these phenomena and to fill the void existing in the literature. Uziel Landau, as a subtopic to his doctoral research,[3,4] has made exploratory experiments on the effect of small wire protrusions on the surrounding

deposit. It is proposed in this project to study the morphological changes induced by the presence of a protrusion as a function of the interrelated parameters current density, overpotential, and flow rate by means of scanning electron microscopy, optical microscopy, and surf-analysis.

The complexity of the hydrodynamics in turbulent flow around a protrusion preclude an analytical solution of the velocity profile and the corresponding mass transfer problem. Levich[5] discusses qualitatively the flow around a protrusion in a laminar stream. White[6] after Johnston[7] shows the three dimensional boundary layer arising from the secondary flow against a cylindrical obstacle as illustrated in Fig. 1. Experimental studies have dealt with the formation of eddy trains, and their onset and stability behind such shapes as cylinders, cones, wedges and spheres in unbounded turbulent flow. The symmetry and unboundedness of the flow in these experiments prohibit the direct application of their results here.

Morphological studies of the deposition of zinc,[8-10] gold,[11] and copper[12-14] have been made on highly polished single crystals and grains. Ibl has performed experiments on the formation of powder deposits at and near the limiting current.[11-13] These experiments provide intuitional aids to understanding the deposits obtained under the hydrodynamic and substrate conditions utilized in this study.

In addition to observations of the deposit around protrusions it was possible to record surface morphology trends in the undisturbed regions of the electrode on both mechanically and electrochemically polished substrates as current, overpotential, and flow rate were varied.

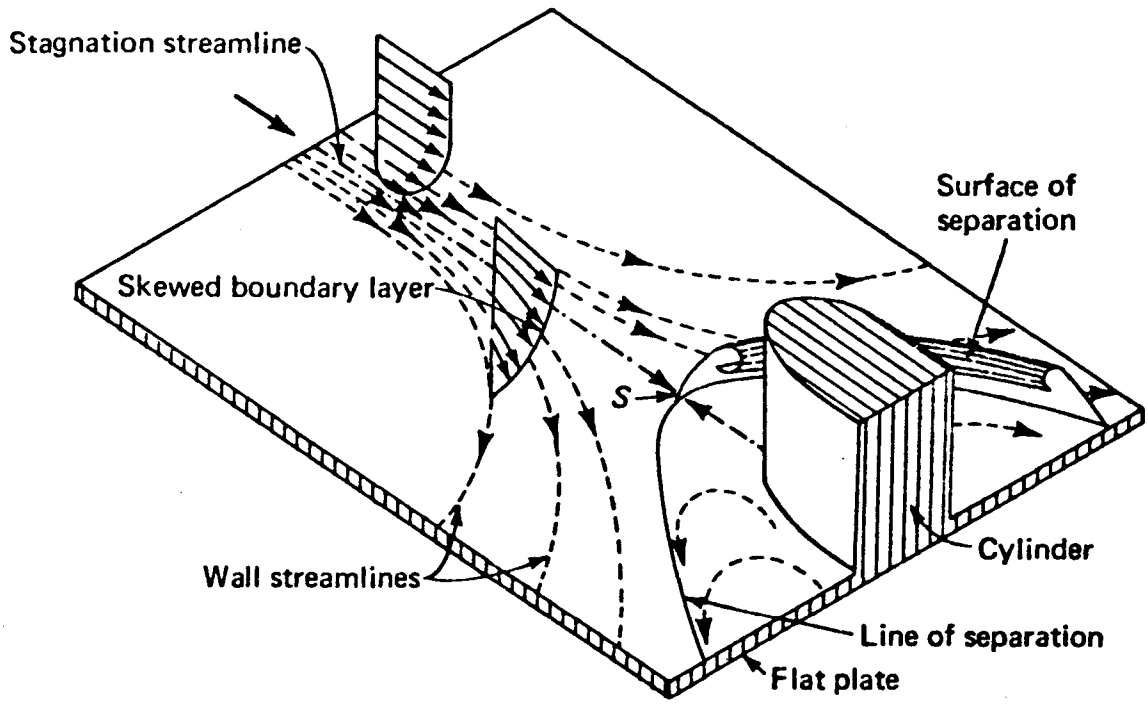

Fig. 1. Three-dimensional separation in flat plate flow against a cylindrical obstacle (from F. M. White[7]).

II. EXPERIMENTAL

2.1. Flow System and Peripheral Equipment

The flow system, electronic equipment, and electrode assembly used in these experiments were those designed and built by Jan Selman and Uziel Landau[3] in this laboratory. The electrolysis channel with 2.3 cm electrode separation (hydraulic diameter 4 cm) was made up of a 7 cm wide and 40 cm long segmented cathode with two 4 cm wide coplanar side segments, faced by a 40×15 cm anode. A entrance region was provided so the hydrodynamic boundary layer would be fully developed in the electrode region. Laminar to highly turbulent flow (up to Reynolds number 120,000 for Schmidt number of 1000) was obtainable. Both galvanostatic and potentiostatic experiments were possible with a maximum current of 100 amperes. A Vidar data acquition system and Ampex tape drive were used to monitor the flow rate from magnetic flow meters, total current, total IR drop and the segmental currents and overpotentials. X-Y and X-t recorders were used to visually monitor one segment during the experiment. Figures 2 and 3 show the general layout of the system. Further details are provided in the doctoral dissertation of U. Landau.[3]

2.2. Electrode Modifications

The electrodes, made of OFHC copper, had to satisfy the following criteria: (1) fit in the existing cathode holder; (2) have a reusable and reproducible surface; (3) be compatible with the analytical equipment used, and (4) yield the maximum amount of useful data per experiment.

The electrode shown in Fig. 4a and 4b was used for the observation of wakes behind wires and spheres on the surface. A compression fitting made up of a teflon cone and separate tightening screw, as shown in Fig. 4b,

ELECTRODEPOSITION AROUND PROTRUDING SURFACE IMPERFECTIONS IN TURBULENT FLOW

Contents

Abstract v

I. Introduction 1

II. Experimental 4

2.1. Flow System and Peripheral Equipment 4

2.2. Electrode Modifications 4

2.3. Electrolyte 10

2.4. Electrode Preparation 10

2.5. Mode of Operation 12

2.6. Analysis of the Results 14

2.7. Quantitative Comparison of the Amount of Deposit Inside and Outside the Wake 16

A. Electrode 16

B. Preparation 16

C. Analysis 16

III. Results 18

3.1. Deposition Around Protrusions 18

A. Photographs 18

B. Dimensions of the Wake 22

C. Surf-Analysis 28

D. Quantitative Comparison of the Amount of Deposit Inside and Outside the Wake 36

E. Wake Cross-Section 39

3.2. Surface Morphology 39

A. SEM Micrographs of the Deposit 39

B. The Effect of Overpotential and Substrate on the Deposit Morphology 43

3.3. Additional Results 48

IV. Discussion 49

4.1. The Wake 49

A. The Macro-Scale 49

B. The Micro-Scale 51

C. Wakes Around Gas Bubbles 57

4.2. Surface Morphology 58

V. Future Work 59

Nomenclature 61

Acknowledgements 62

Appendix 63

References 66

ELECTRODEPOSITION AROUND PROTRUDING SURFACE IMPERFECTIONS IN TURBULENT FLOW

Eric John Carlson

Inorganic Materials Research Division, Lawrence Berkeley Laboratory and Department of Chemistry; University of California, Berkeley, California 94720

ABSTRACT

Cathodic deposition of copper around small cylindrical and spherical protrusions located on the cathode surface in a channel with rectangular cross-section (D_h = 4 cm) at Reynolds numbers up to 50,000 was studied as a function of the protrusion height and diameter and of the related parameters of flow rate, overpotential and fraction of the limiting current. The distinctive wake region, caused by perturbations in the flow induced by the protrusion, was characterized using scanning electron microscope, optical microscopes and macrophotography. These techniques and quantitative measurement of the amount of deposit in- and outside the wake revealed:

1) The current density inside the wake was approximately twice as high and the porosity four times larger than those outside.

2) The wake was not reflected in the deposit when the height of the protrusion was below 0.1 mm and when $i/i_L \leq 0.9$.

3) At the limiting current large powder clusters formed in the wake in contrast to the uniform powdery growth outside the wake.

The above observations are explained in terms of mass transfer control of the deposition process. The hydrodynamic changes, induced by the protrusion, thin the boundary layer causing an increase of limiting

current density (i_L) and of total current (I). As the mass transfer boundary layer thickness (δ_M) decreases, it approaches the order of the amplitude of the roughness (h) and deposition occurs over the entire profile ("3-dimensional growth"). Outside the wake where $\delta_M > h$ preferential deposition occurs at peaks and growth proceeds vertically ("1-dimensional growth"). Below the limiting current surface overpotential dominates and a more even current distribution results.

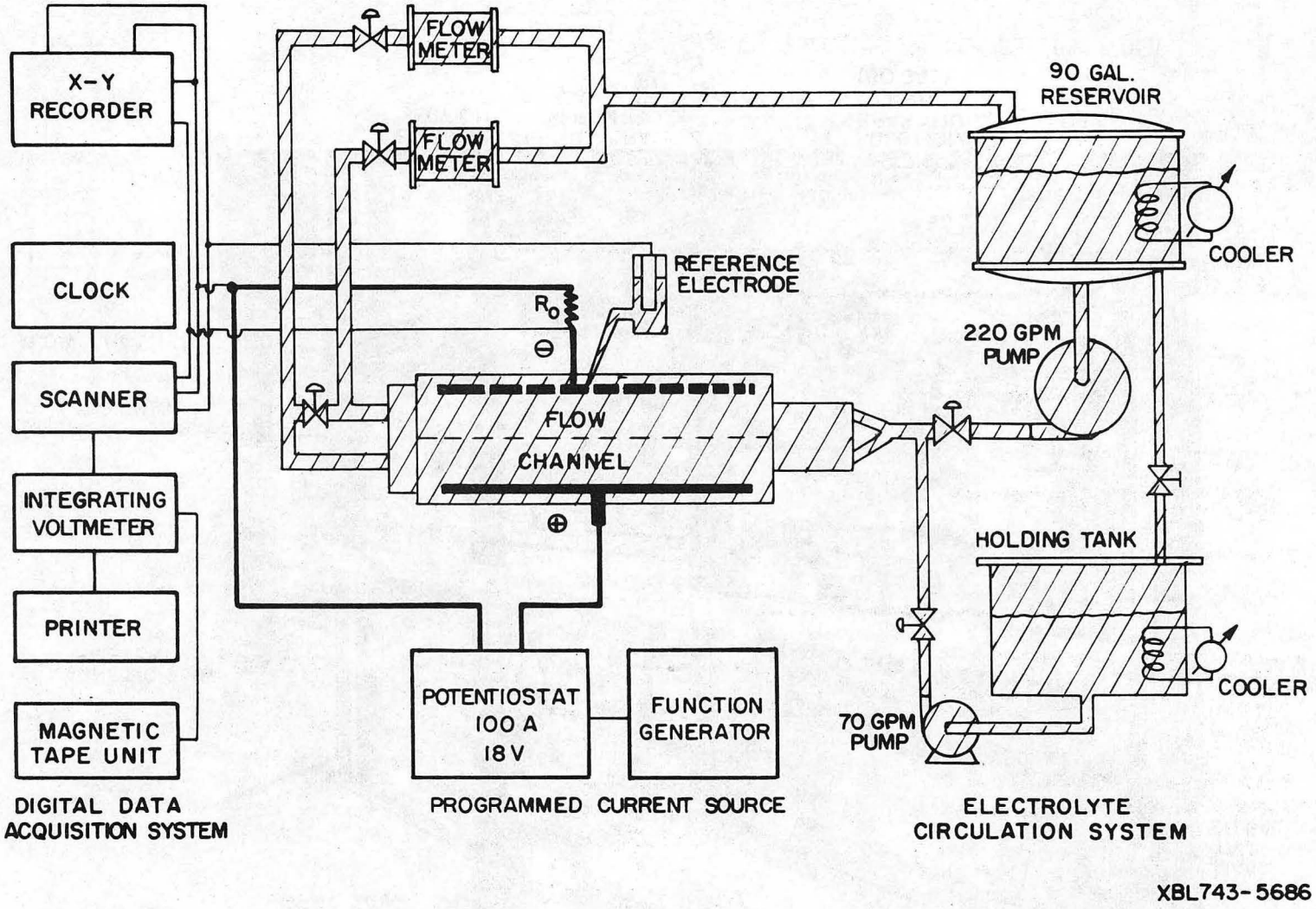

Fig. 2. Schematic of the experimental system (U. Landau's thesis[3]).

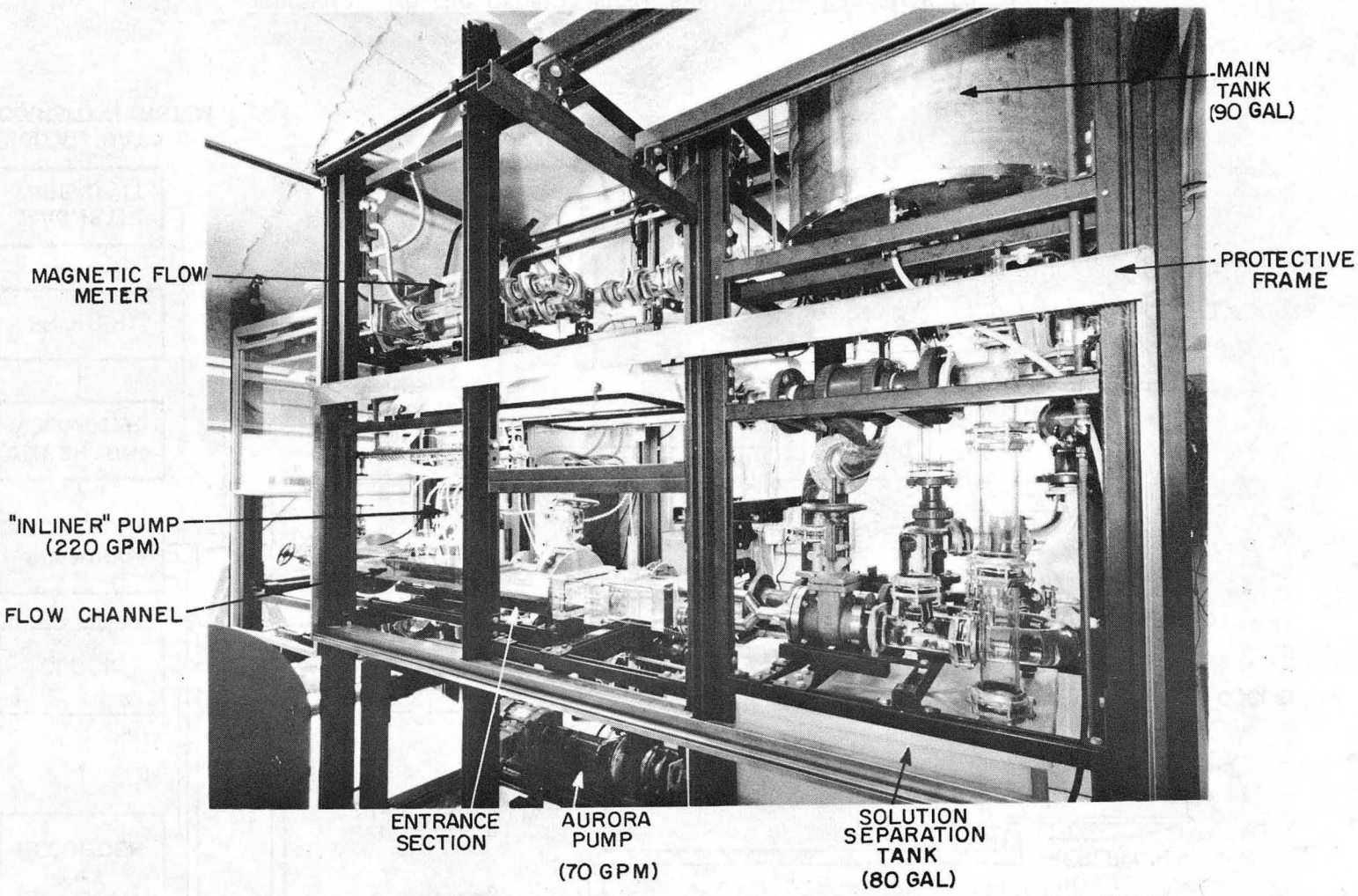

Fig. 3. Photograph of the flow system (U. Landau's thesis[3]).

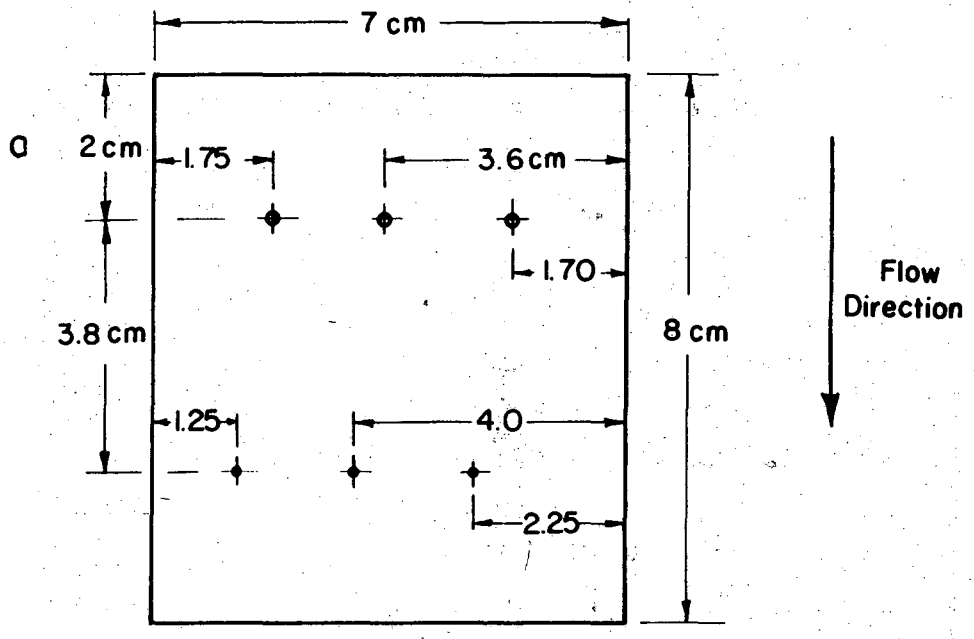

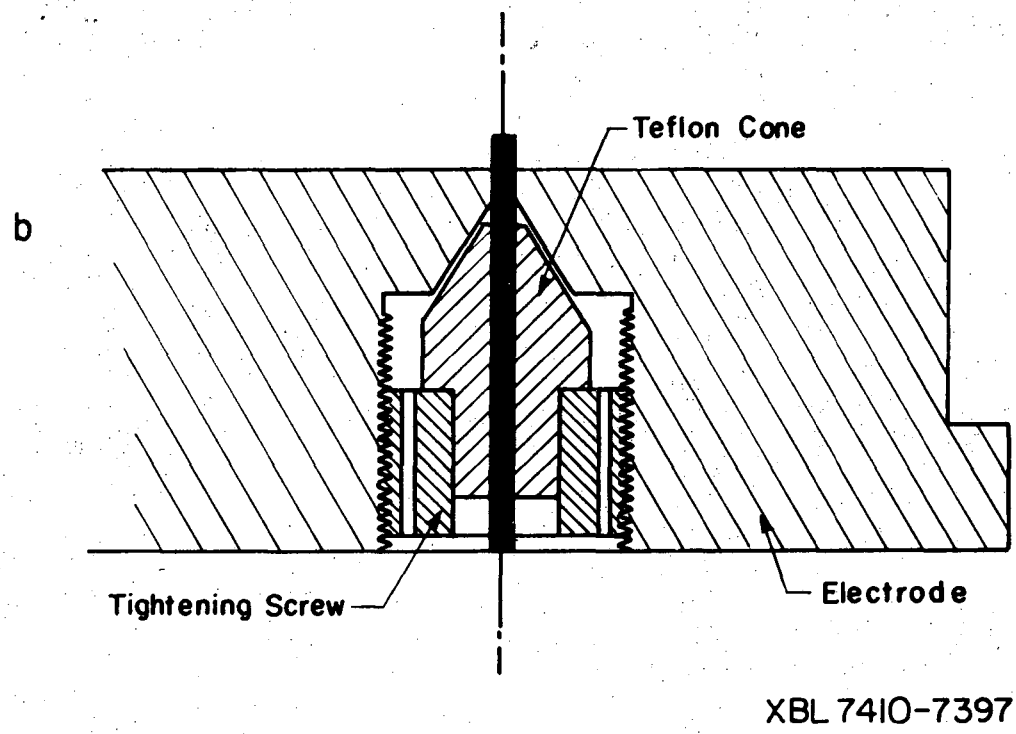

Fig. 4. a. Location of wire protrusions on electrode.
b. Side-view of swagelock assembly holding a wire protrusion.

enabled the height of the wire protrusions to be varied. Six of these fittings were machined in the electrode in two rows, using two different diameters (0.65 and 0.30 mm), with the centerlines aligned so that the wakes of the downstream wires would not interfere with the remaining ones. In this manner both the effect of diameter and height could be examined simultaneously. Spheres made by welding techniques on the end of a copper wire were placed on the surface of the electrode by drawing the wire through the hole from above the electrode until the sphere rested on the surface. The best spherical shape is obtained for sphere diameters twice that of the wire. Both inert spheres and wires (non-conducting protrusions) were made by dipping the objects in acrylic diluted with acetone.

Electrode inserts, 1.5 in. by 1 in. and 1 in. by 1 in., with a corresponding slot in the channel electrode as shown in Fig. 5a were made for use in the scanning electron microscope. After the entire electrode was mechanically polished one of the segments was removed and further polished electrochemically. Having both segments with different surface preparation adjacent to each other during the same experiment made possible the simultaneous post mortem observation of deposition on a electropolished and mechanically polished surface. These segments were also modified for use with the cylindrical and spherical protrusions. A simplified compression fitting consisting of a Teflon plug with threads was used to hold and position the wire. The fine structure of the wake could then be observed by placing these electrodes in the SEM. As will be described later, these segments were embedded in "Bakelite" and sectioned to obtain side views of the deposit in the wake. In a repetitous

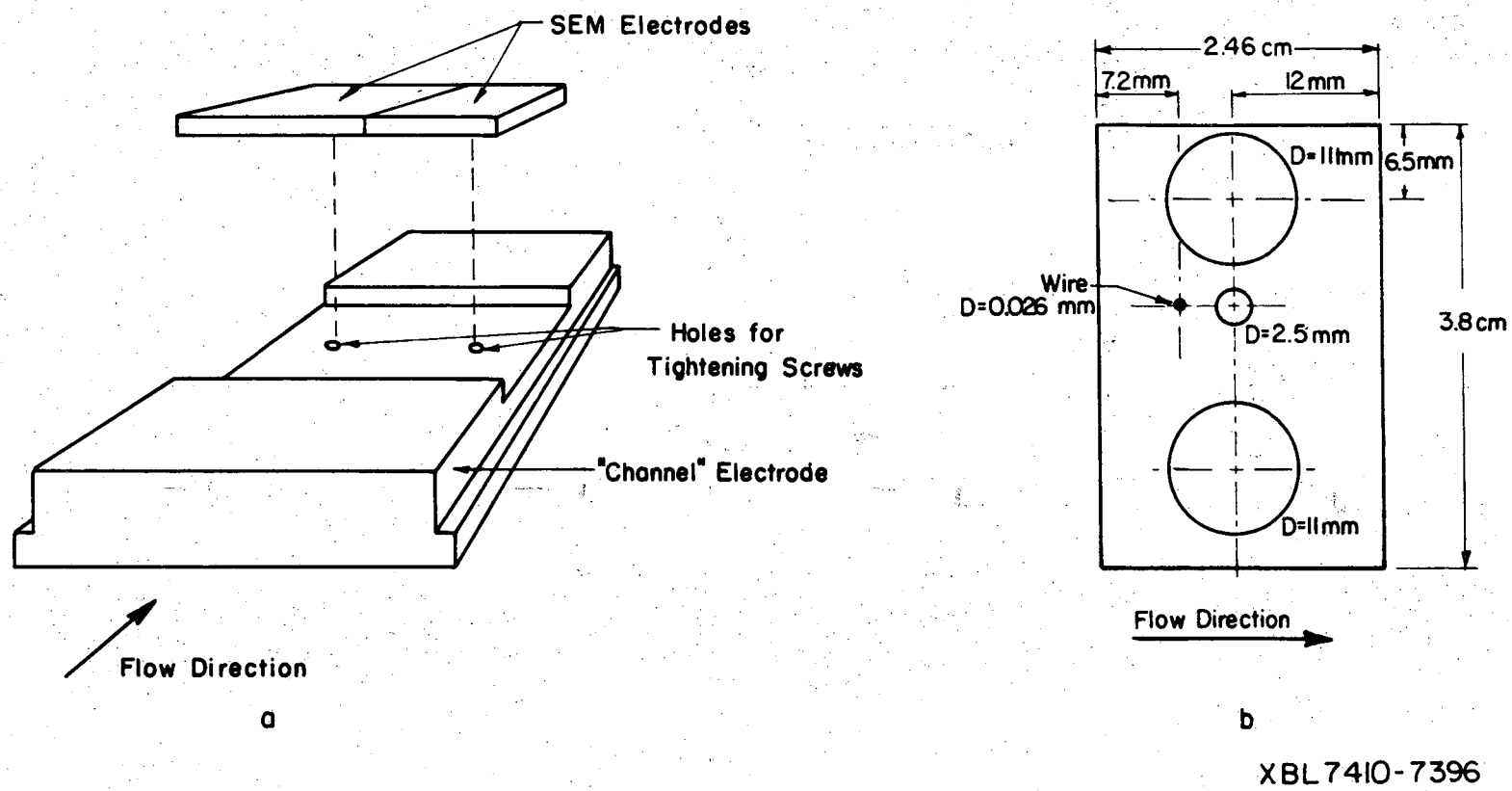

Fig. 5. a. Position of SEM electrodes in the channel electrode.
b. Location of the discs on SEM electrode used in determining the amount of deposit inside and outside the wake.

study of this kind, time and money were saved by using a small removable segment of the electrode.

The electrodes described in the preceeding two paragraphs could be positioned at or near the trailing edge of the channel where the undisturbed mass transfer boundary layer reaches it's asymptotic thickness. The current and overpotential in this region for unperturbed flow are uniform, consequently variations in the deposit can, therefore, be assigned entirely to the presence of the protrusion.

2.3. Electrolyte

The two solutions used contained A.R. grade copper sulfate, sulfuric acid and glycerol. The acid concentration was determined by titrating with sodium hydroxide and the copper sulfate concentration by electrogravimetery using platinum gauze electrodes. The glycerol concentration was not determined directly but characterized by the Schmidt (ν/D) number.

Integral diffusion coefficients were determined using a rotating disk electrode. The kinematic viscosity (ν) was found with Ubbelohde type viscometers.

The physical parameters for solution A and B are summarized in Table I.

2.4. Electrode Preparation

The set of electrodes were handpolished in a "jig" to maintain a flat surface. The entire surface was polished using successively finer grades of silicon-carbide and emery paper down to 4/0 grit. Furthermore, before electropolishing, segments were mechanically polished with 1 μ diamond paste on a polishing wheel, then electropolished with a phosphoric acid, ethanol, propanol, butanol and dextrin solution as described by Ibl.[16] Oxide films were removed in a bath consisting of

Table I. Physical parameters of the electrolyte.

Solution	(moles/liter) c_{CuSO_4}	(moles/ℓ) $c_{H_2SO_4}$	(cm^2/sec) $D\times10^6$	(cm^2/sec) ν	$Sc(\nu/D)$
A	0.029	1.32	2.07	0.022	10390
B	0.021	1.04	3.82	0.018	4620

40 ml conc. HCl (ρ = 1.19 g/cm^3), 1 L CH_3CH_2OH, and 40 g $SnCL_2 \cdot 2H_2O$.[18]

The experiments with protrusions were prepared in a similar manner except the wires were initially positioned with their tops slightly above the surface so that polishing would produce a flat, level surface. When the polishing was completed the wire was again extended above the surface to clean off any burrs on the edges. Then using a microscope with a micrometer dial on the fine focusing knob the heights were adjusted. In a number of experiments small strips which were positioned parallel and transverse to the wake were coated with acrylic to provide a reference line corresponding to the substrate so the deposit thickness could be determined with the surfanalyzer.

2.5. Mode of Operation

In a galvanostatic experiment the total current remains constant. As the surface area increases there is a decrease in the local current density, i, which under the simplest conditions will be inversely proportional to the area. This corresponds to the case in which the mass transfer boundary layer conforms to the surface topology. If this is not the case, deposition will occur preferentially on the peaks because of the shorter diffusion length and spherical diffusion. For this case no accurate statement can be made describing the change in i except that on the average it will decrease. The picture is further complicated by no longer having a uniform limiting current over the entire surface as the surface roughens.

In potentiostatic experiments the total current is allowed to vary in order to maintain the total overpotential, the sum of surface (η_s) and concentration (η_c) overpotential, constant. If the hydrodynamic

conditions remain constant, as in the case of a smooth deposit, and the total current (I) increases proportionally to the surface area increase, so as to maintain the local current density (i) constant, then i/i_L will not change.

In both potentiostatic and galvanostatic experiments the surface conditions can not be maintained constant because as deposition takes place the "substrate" changes. (As soon as a monolayer is deposited the solution no longer "sees" the polished substrate and the kinetic parameters will, therefore, change.) The experiments were operated in the potentiostatic mode because this offered the best means of maintaining the local current density (i) constant and as a consequence, η_c and η_s.

The overpotential on the ideal limiting current plateau increases until a successive reaction occurs and the current can increase. While operating at the limiting current, the overpotential must be specified so as to unambiguously locate the point of operation on the I vs η_T curve. In actual experiments the "plateau" is sloped thereby obscuring the exact value of the limiting current. The experiment was brought to the initial operating point in a potentiostatic ramp. (For different flow rates operation at the same total overpotential does not imply that η_c and η_s are the same for each experiment.)

The number of coulombs, the total amount of copper deposited was kept approximately constant for each experiment. As a consequence, for a given overpotential the low flow rate experiments were of longer duration. Very long deposition times are undesirable because of the possible initiation of dendrites as described by Bockris.[19] To avoid unsteady state effects the current was brought to its final value

by a ramp of approximately 3 min duration. The length of the high flow rate experiments at the limiting current was approximately 20 min, therefore, the ramp time did not comprise a significant portion of the experiment.

2.6. Analysis of the Results

In order to present a qualitative picture of the morphological changes corresponding to different deposition conditions extensive use was made of photographs from a scanning electron microscope (SEM), metallographic microscopes, and macrophotography.

The SEM used was a model JSM-U3 (Jeol Japan Electron Optics Laboratory Co., Ltd) and as set up had a upper useful magnification of 10,000×. As previously explained, the electrodes were designed to fit in an existing sample holder of the SEM so that the magnifications indicated on the instrument dial would remain valid. Photographs were made using Polaroid Type 55 P/N at an aperture of f8 and at two angles of inclination, 0° and 30°. It was necessary to tilt the smoother samples to increase contrast and improve the resolution. Often entirely new and revealing features were observed when the sample stage was tilted as illustrated in Fig. 22b and 22d. For the rougher samples the large depth of field of the SEM offered a tremendous improvement in resolution and magnification compared to optical microscopes.

In addition to the SEM the Unitron Metallographic (Model U-11) and Zeiss Ultraphot II microscopes were used. The Ultraphot was used with oil immersion lenses to obtain micrographs (1000×) of cross-sectional views of the wake. The Unitron which was located in the laboratory was used for low magnification (50×) views. The roughness of the surfaces involved and the limited depth-of-field of these microscopes restricted their use.

To record the general characteristics of the wake the MP-3 Polaroid Land Camera with a macrolens and bellows was used to take 10× photos of the protrusions on 4×5 Polaroid Type 47 and Kodak Tri-X Professional Sheet Film.

A Clevite Gould surfanalyzer Model 150 with a probe of the following specifications:

50 mg stylus force

Linear stylus displacement ±0.004 in.

R = 0.0001 in.

Diamond

was the last method used to characterize the deposit. By removing the protrusions from the surface the probe could be run through the centerline of the wake far into the tail and normal to the centerline in the region around the protrusion. Making parallel and transverse scans through different portions of the wake yielded a quantitative picture of the relative changes of height in the wake. The absolute thickness of the deposit was determined by masking portions of the electrode with acrylic parallel to the wake and then running the surfanalyzer probe through these two strips after the acrylic had been removed with acetone.

The SEM electrodes were sectioned by encasing them in Bakelite. The Bakelite in powder form was poured around the electrode in the chamber of the press, then melted and allowed to set at 2 tons pressure for 5 min. After cooling, the electrode, now in a cylindrical plug of Bakelite, was placed in a mill and machined to within 0.010 in. of the desired cross-section. This surface was then polished down to 1 μ. In this way material from machining was removed and a flat surface obtained.

The limited depth of field of the microscope at 1000× necessitated obtaining a flat surface.

2.7. Quantitative Comparison of the Amount of Deposit Inside and Outside the Wake

A. Electrode

A stainless steel (304) SEM electrode was made with removable discs located in the positions indicated in Fig. 5b. The large discs are well outside the wake and provide a sample of the deposit in the undisturbed region of the electrode. The small disc is located directly behind the protrusion in the far-wake. Stainless steel was used so that the copper deposit could be stripped with HNO_3 for the analytical tests and then reused.

B. Preparation

The set of electrodes were polished in the manner previously described with the SEM electrode receiving additional polishing with 1 μ diamond paste. Polishing removed any differences in height between the discs and the main electrode. The copper wire protrusion was then pushed above the surface. Immediately prior to placing the electrode holder in the channel the stainless steel electrode was cleaned with a 30% HCl solution to remove the passive layer.

C. Analysis

After removal of the discs from the electrode and rinsing with distilled water the discs were sent to the analytical laboratory* where

*Tom Morrison, Research Associate III, UCB College of Chemistry Analytical Laboratory.

the copper was removed with 8N HNO_3. The weight of copper per disc, was determined by complexing the copper with excess ammonia and then by performing an analysis of the concentration by light absorption with a Beckman spectrophotometer at 360 mμ.

III. RESULTS

In the following sections, observations of the wake resulting from cylindrical and spherical protrusions and the surrounding morphological changes are presented in the form of macrophotographs, surf-analysis profiles, and SEM and optical micrographs. As often as possible all of these techniques were applied to the same sample so as to provide an increasingly refined view, ranging from the macro(10×)- to the microscale(10,000×). It is hoped that a presentation of this form will allow the reader to keep all parts of the composite picture in perspective.

3.1. Deposition Around Protrusions

A. Photographs

The macrophotographs in Figs. 6 and 7 illustrate the general characteristics of the wake formed around cylindrical and spherical protrusions. The microstructure (~2μ) observed inside and outside the wake with the SEM will be presented in Section 3.2 (surface morphology). Table II lists the conditions of deposition for each series of photographs. Surf-analysis profiles, Section 3.1-C, of the wakes shown or of similar experiments provide quantitative values of the relative height differences between the wake and surrounding deposit. A comparison of the amount of deposit per unit area in these regions is given in Section 3.1-D.

Figures 6 and 7 show how overpotential (or fraction of the limiting current), and the height and diameter of the cylinder affect the wake. For high overpotentials (~-400 mV) a powdery deposit in the wake region, as shown in Figures 6a and 7a, clearly differentiate the wake from the rest of

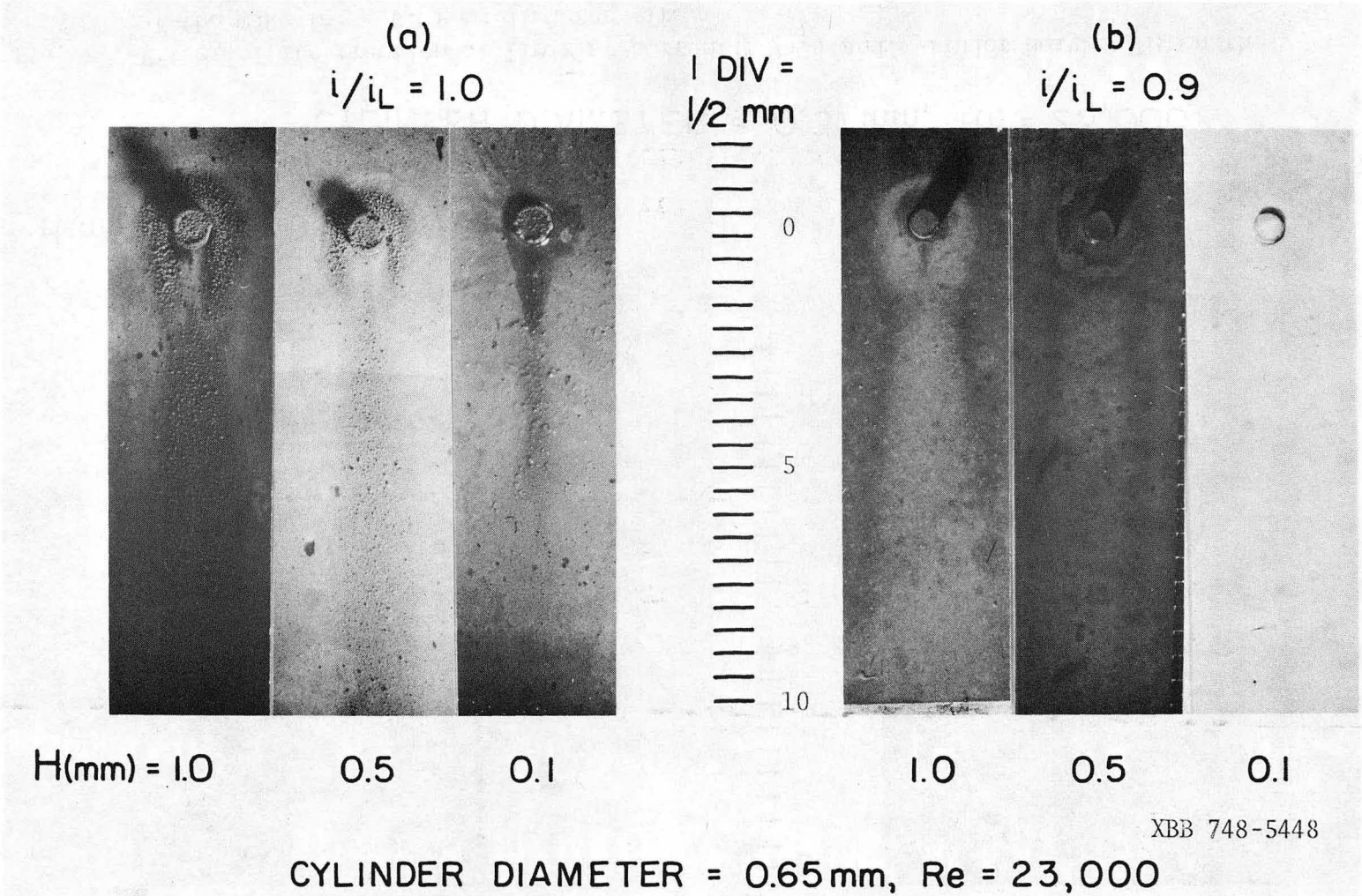

Fig. 6. Effect of the fraction of limiting current (i/i_L), and cylinder height (H) on the form of the wake for a 0.65 mm diameter wire.

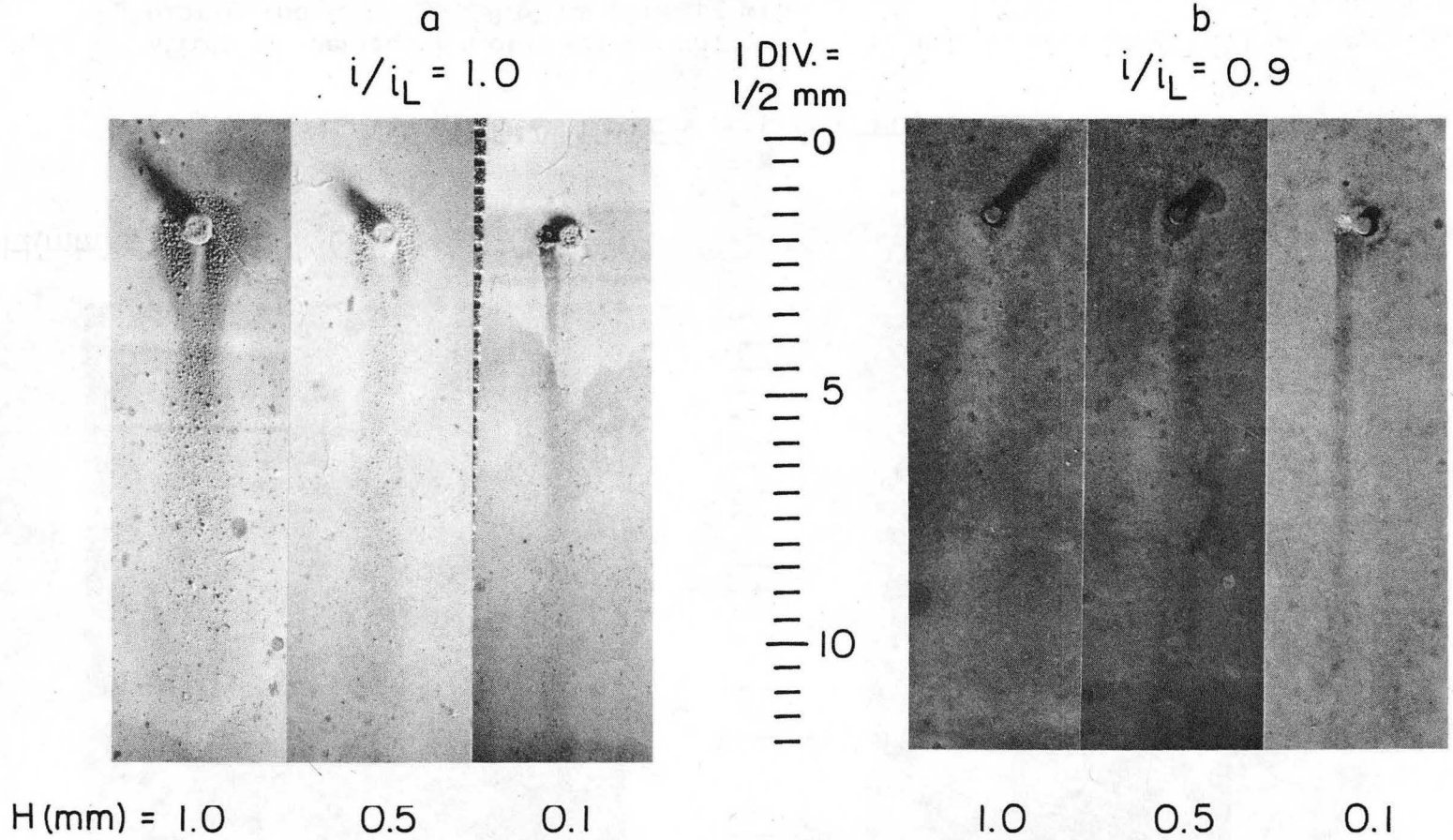

Fig. 7. Effect of the fraction of limiting current (i/i_L) and cylinder height (H) on the of the wake for a 0.31 mm diameter wire.

Table II. Experimental Parameters for Figures 6-9.

Figure	Re #	i/i_L	$-\eta$(mV)	mA/cm^2 $\langle i \rangle$	(min) Duration	Solution
6a, 7a	23,000	1	450	~7.0	15.0	A
6b, 7b	23,000	0.9	190	~6.3	16.6	A
8	28,000	1	350	~11.0	20.0	B
9	23,000	1	450	~7.0	15.0	A

the electrode. As the overpotential decreases the wake became less distinguishable from the surrounding deposit as shown in Figs. 6b and 7b, and at -150 mV was non-existent. The exact point of disappearance was not determined because experiments were performed at only three over-potentials (-400, -300 and -150 mV).

Figure 8 shows the wake formed at Reynolds number of 28,000, η = -350 mV, and 10.8 coulombs/cm^2. The SEM blowup of the top of the cylinder illustrates the effect of the flow and higher current density at the edge had on the deposit. The deposit was increased around the edge with the front half receiving still more deposit than the rear.

The wakes formed around spheres, as shown in Fig. 9, did not differ in over-all appearance from those of the cylinders. An additional area of powdery deposit does appear immediately behind the sphere. The surf-analyzer results, presented later, revealed significant differences on a micro-scale which occurred around the sphere. No difference could be detected in the wake from conducting spheres when inert spheres coated with acrylic were used in the same experiments.

B. Dimensions of the Wake

The dimensions of all the wakes shown are summarized in Tables III and IV. As the height and diameter of the protrusion decreased so did the dimensions of the wake. The size of the wake did not change noticeably as i/i_L was decreased to 0.9.

At a Reynolds number of 30,000 for solution B the mass transfer boundary layer (δ_M) is approximately 15 μ and the laminar sublayer and turbulent core are 100 μ and 600 μ respectively. (Equations and the assumptions used to obtain the above values are given in the Appendix.)

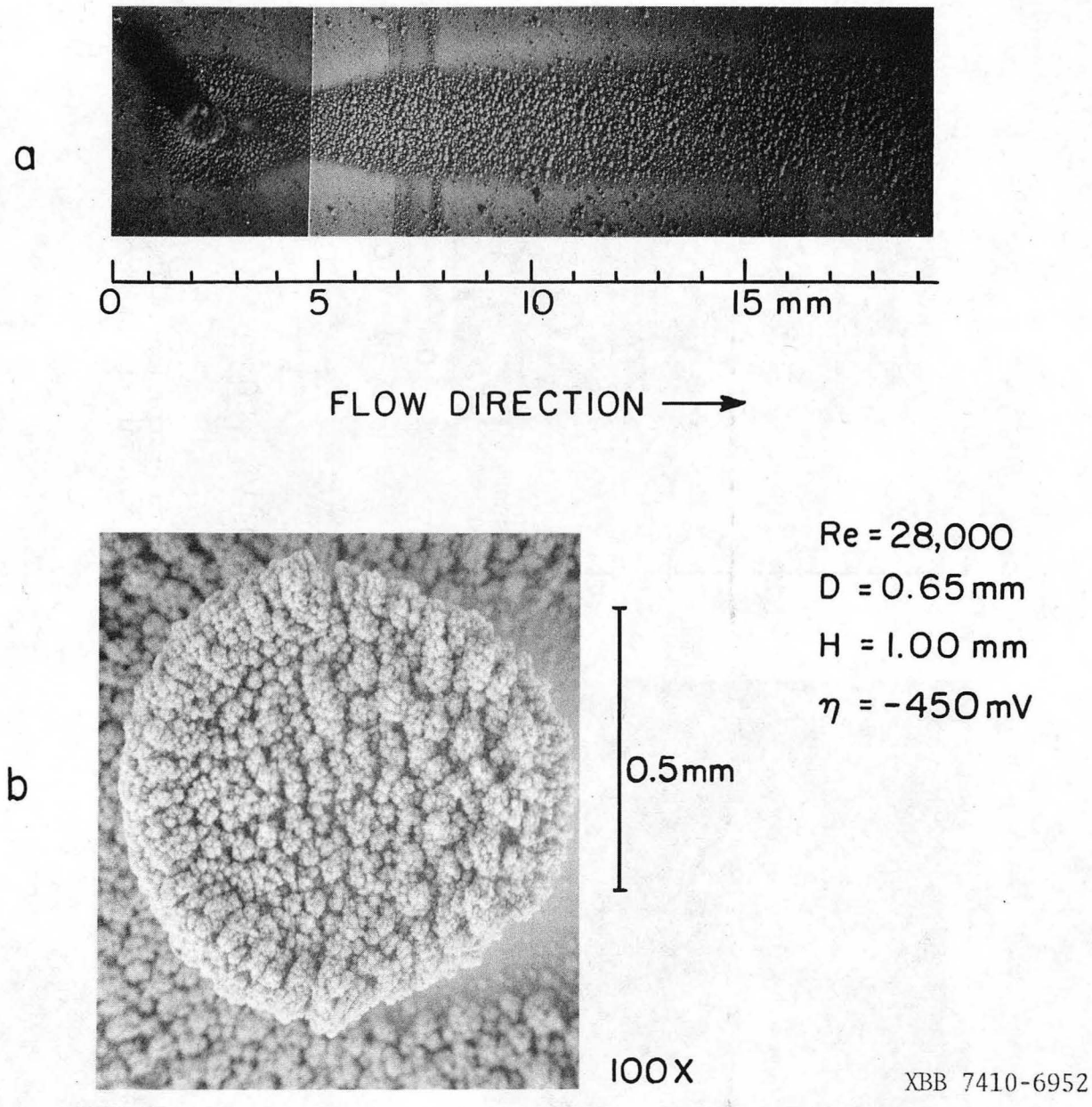

Fig. 8. a. Composite photograph showing more of the far-wake. (Vertical bands across the wake are from insulating strip of acrylic.)
b. SEM micrograph, top of wire, showing preferential deposition around edge and front of the wire.

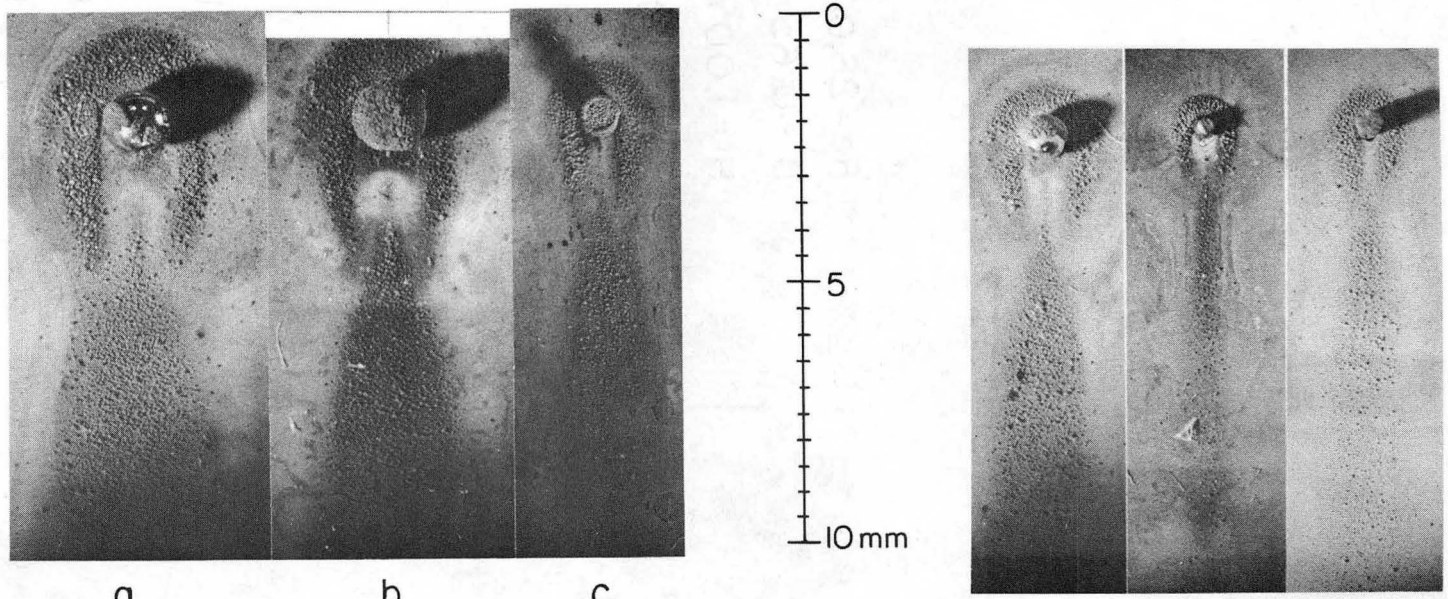

	a	b	c	a	b	c
D(mm)	1.30	1.30	0.65	0.62	0.31	0.31
H(mm)	—	—	1.00	—	0.50	1.00

Re = 23,000; $i/i_L = 1.0$

XBB 7410-6951

Fig. 9. Conducting and nonconducting spheres compared to wire protrusions. The acrylic coating did not completely cover the nonconducting spheres resulting in the spotty deposit on the surface of the protrusion.

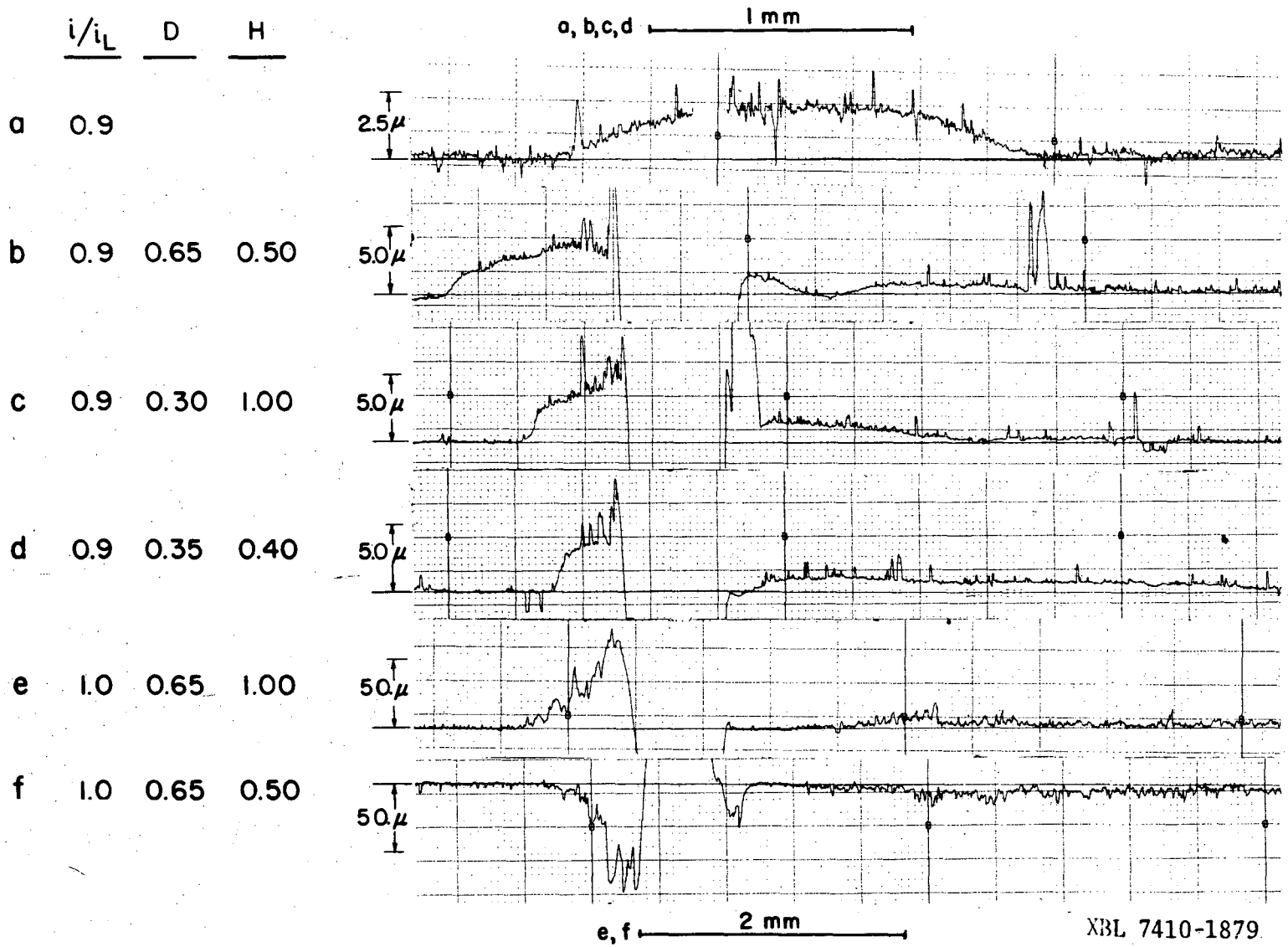

Fig. 10. Surface profiles through the centerline of the wake of protrusions similar to those shown in Figs. 6 and 7. Profile a was made normal to the centerline in the far-wake. (Note that the vertical scale of profiles e and f is 10× that of the others.)

Table III. Dimensions of the wakes in Figs. 6 and 7.
a. Width of the wake through the diameter of the wire.
b. Distance between inside edges of the pincer-like tails.
c. Length of the wake surrounding the wire measured through centerline from front of the wake to the tip of the tails.
d. Maximum width of the far-wake.
e. Distance from center of the wire to the leading edge of the wake.

(All dimensions in mm.)

i/i_L		Large Wire (D = 0.65 mm) H = 1.0	0.5	0.1	Small Wire (D = 0.30 mm) 1.0	0.5	0.1
1.0	a	2.1	1.3	0.1	1.5	1.15	0.6
	b	0.6	0.75	-	0.35	0.5	-
	c	2.65	1.35	-	1.75	1.5	-
	d	1.7	1.3	-	1.3	1.7	0.2
	e	1.0	1.35	-	0.65	0.45	-
0.9	a	2.2	1.6	-	1.6	1.25	-
	b	0.6	0.75	-	0.4	0.5	-
	c	2.7	1.8	-	1.9	1.25	-
	d	2.0	1.4	0.8-0.9	1.5	0.95	-
	e	0.95	0.8	0.5	0.6	0.5	-

Table IV. Dimensions of the wakes in Fig. 9. (Data starts with figure on the left and proceeds to the right. Code letters for the dimensions same as Table 3.)

Protrusion	"Inert" Sphere	Sphere	Wire	Inert Sphere	Inert Wire	Wire
H			1.0		0.5	1.0
D	1.30	1.30	0.65	0.62	0.31	0.31
a	3.5	3.3	2.1	2.6	1.2	1.5
b	1.5	1.25	0.6	0.9	0.5	0.4
c	4.4	4.3	2.65	2.8	1.5	1.8
d	3.3	2.5	1.7	1.8	0.5	1.1
e	1.9	1.8	1.0	1.0	0.6	0.8

(All dimensions in mm)

C. Surf-Analysis

Figure 10 contains profiles made parallel to the flow through the centerline of the cylindrical protrusions shown in Figs. 6 and 7. Profile a was made across the far wake. Profiles a, b, c and d are of the wakes formed at low overpotential. The vertical scale of these are 1/10 of that used in profiles e and f, wakes formed at high overpotential. (Note: Profile e is inverted because the surf-analyzer was started in the tail region and moved in a direction opposite of the others. The extremely high peaks adjacent to the holes result when the wires are removed and material is pulled up. Profiles e and f appear compressed in the horizontal direction due to the smaller scale used. The diameter of the hole varies from profile to profile because of the difficulty in aligning the probe with the centerline.) The thickness of the deposit in front of the cylinder, for the same height and diameter wire (profile b and f), but different overpotential is approximately 3μ as compared to 55μ. Profiles b, e and f show the smooth region occurring behind the cylinder and the initial region of the far wake. The other profiles are off center and go through the pincer like tails extending around the rear cylinder.

Figure 11 shows the deposit around a 1.3 mm diameter sphere sitting on the surface. Profiles 1, 2, 3 and 4 were made normal to the direction in the immediate vicinity of the sphere. The approximate position of these are shown on the lower profile made parallel to the flow. The black line through 1, 2, 3 and 4 corresponds to the positions of the lower trace. The wake is larger than those shown in Fig. 10 as a

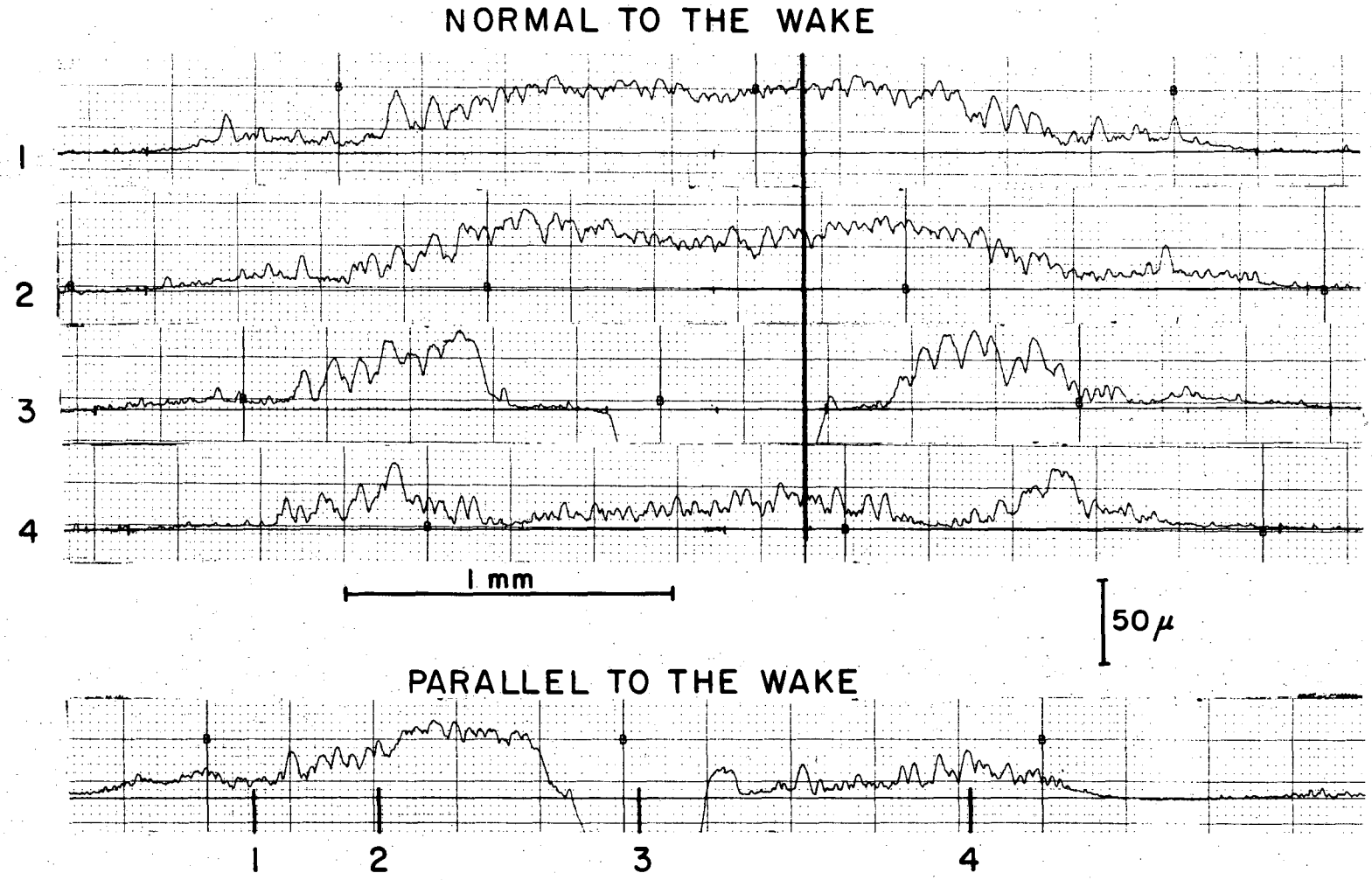

Fig. 11. Profiles made normal to the wake starting in the front of the sphere (D=1.3mm) and moving back in the direction of the far wake. The lower profile made through the centerline of the wake shows the approximate positions of the profiles above as indicated by the numbers.

XBL 7410–1876

consequence of the size differences in the protrusions but, in addition, there are changes in the structure. Around the outer perimeter of the wake a low "plateau" region (~10μ) occurs which then changes to approximately 40 μ closer to the sphere. Profile 3 illustrates how the deposit decreases abruptly under the projected area of the sphere. The diameter of this region equals that of the sphere. In the rear of the sphere between the two pincers of the tail an additional region of powdery deposit occurs. This is shown clearly in profile 4. These features do not appear around the cylinders shown in Fig. 10. Note the symmetry of the profiles about the centerline which indicate that the thermocouple beads approximated a sphere fairly accurately.

Figures 12-15 are surfanalysis profiles of the active and inert spheres shown in Fig. 9. These are shown as further examples and as evidence of the reproducibility of the wakes. Figures 12a and 12b are profiles parallel to the flow and through the hole. These show the beginning of the far wake which was excluded in Fig. 11. Figure 13 shows the relative positions of the traverses contained in Figs. 14 and 15 as indicated by the number adjacent to each profile. No substantial differences occur in the wakes of the active and inert spheres. The profiles could not be made exactly in the same position for different experiments so direct comparisons of the heights are difficult.

Figures 16a and 16b are profiles across the far wake showing the deposit thickness in relation to the substrate. Two strips of acrylic adjacent to the wake provided the reference corresponding to the steps at both sides of each profile. Outside the wake the deposit thickness is approximately 3 μ and inside 30 μ. This does not give any indication

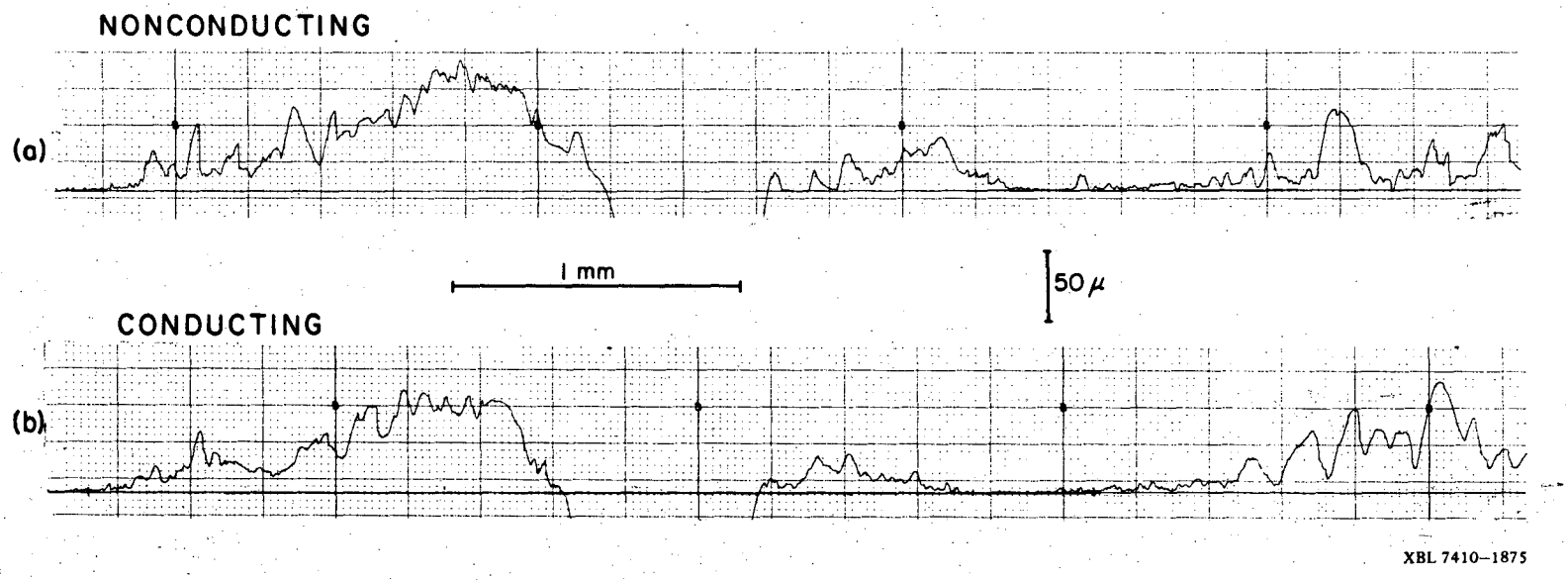

Fig. 12. Profiles made through the centerline of conducting and nonconducting spheres. The beginning of the far wake, not shown in the lower profile of Fig. 11, is shown here.

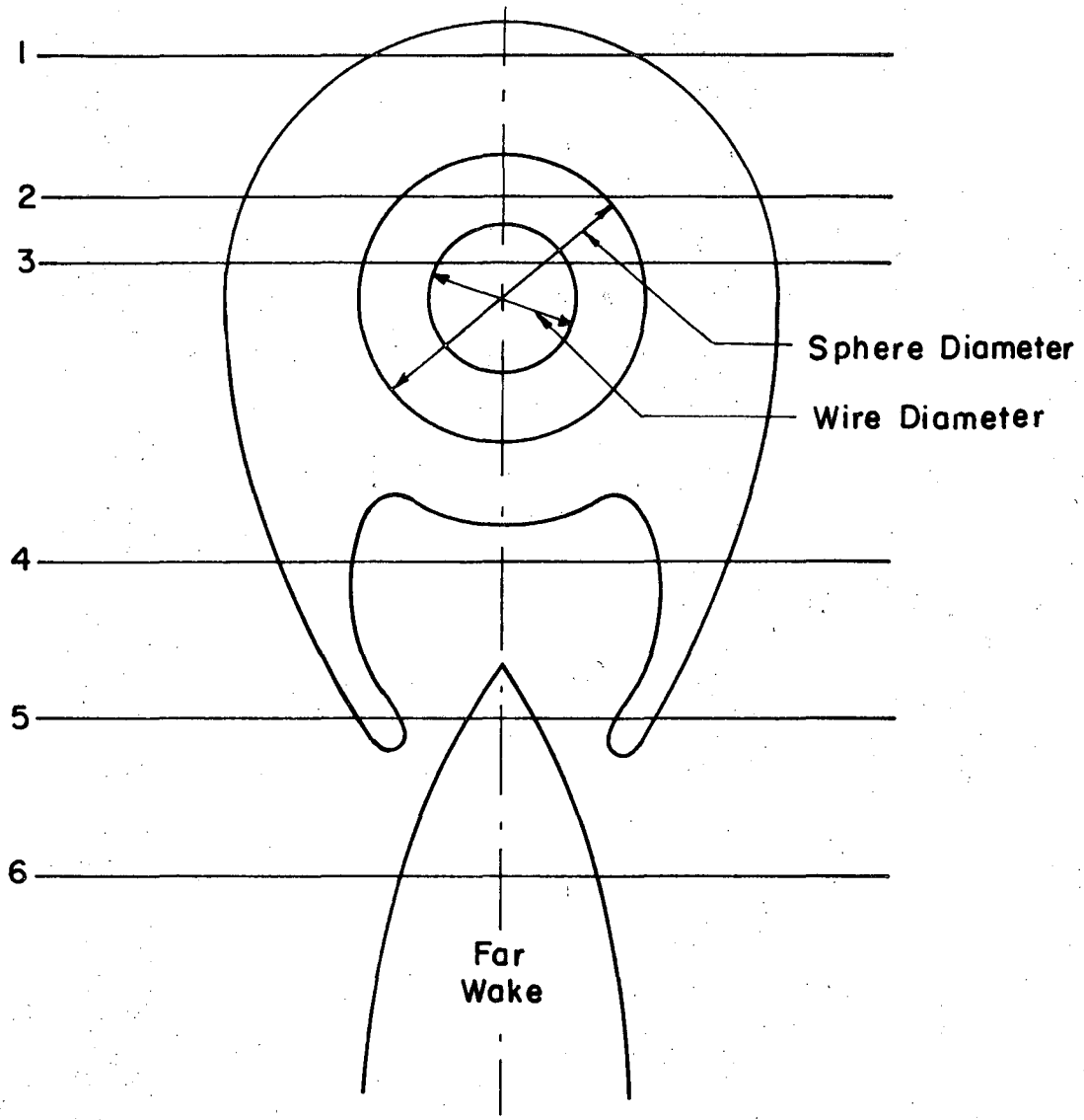

Fig. 13. Schematic representing the form of the wake around the spheres. The numbers and corresponding lines indicate the approximate locations of the profiles presented in the next two figures.

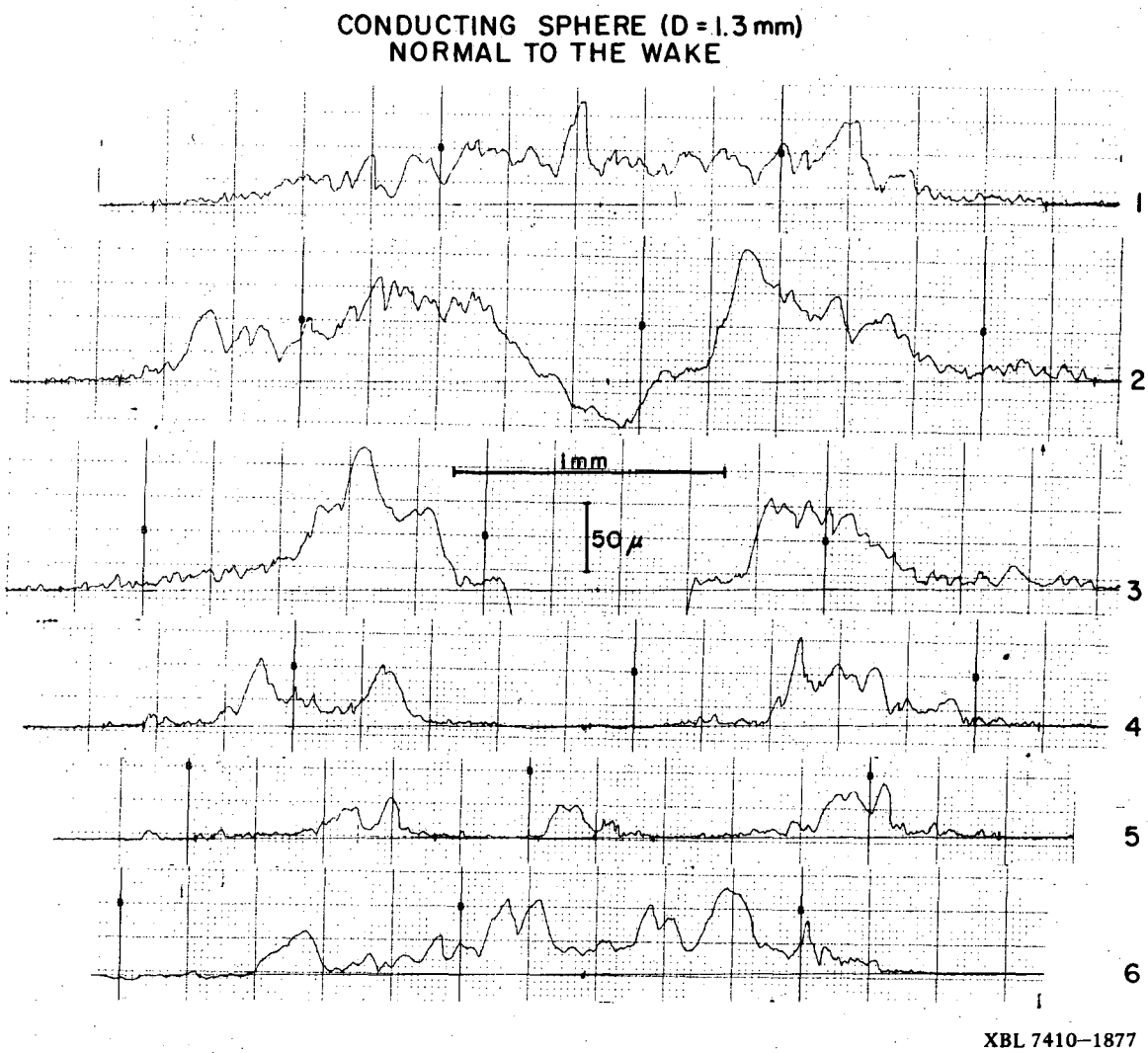

Fig. 14. Profiles made normal to the centerline of the wake around a conducting sphere. The respective position of each profile is given in Fig. 13.

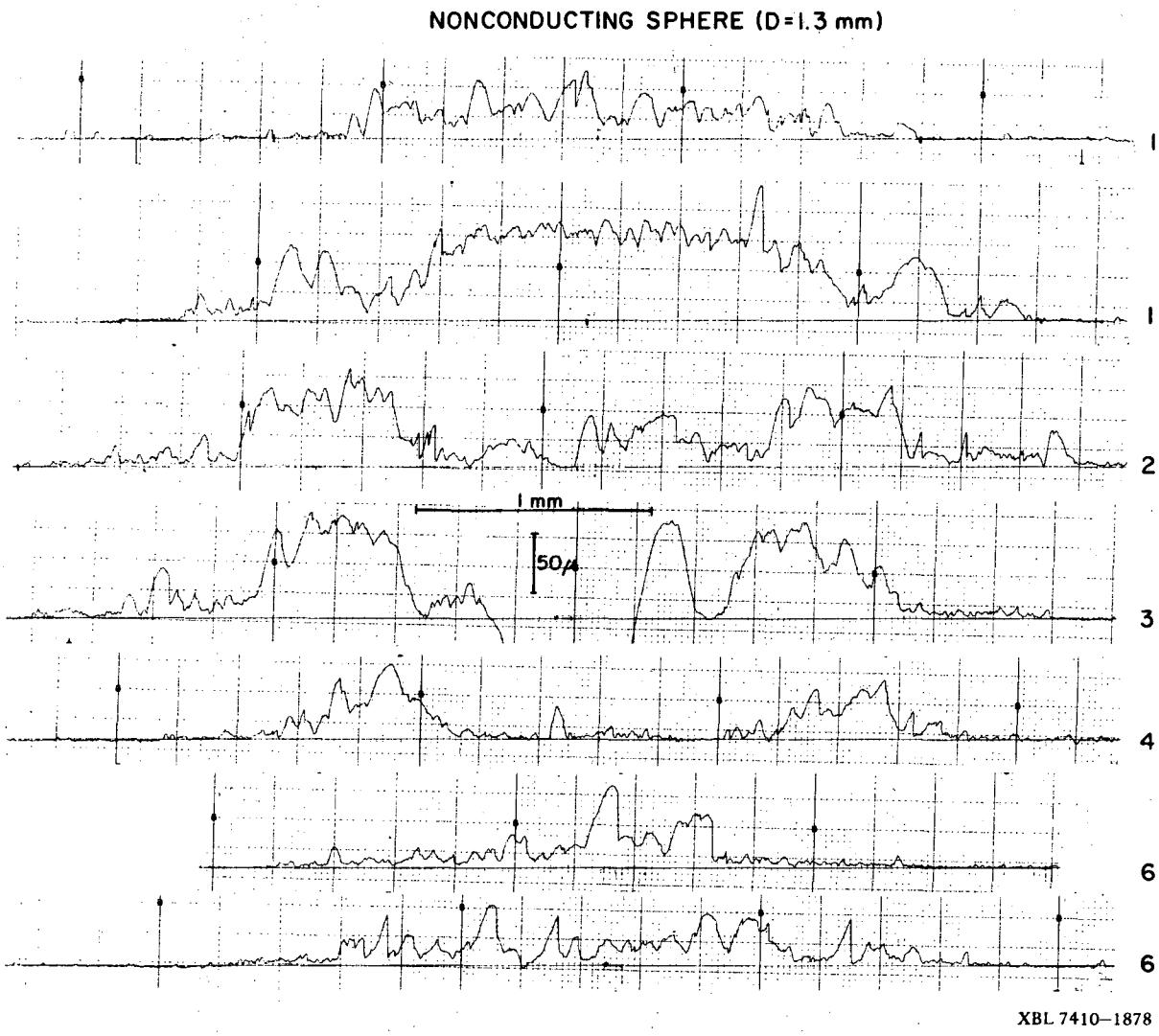

Fig. 15. Profiles made normal to the centerline of the wake around a nonconducting sphere. The respective positions of each profile is given in Fig. 13.

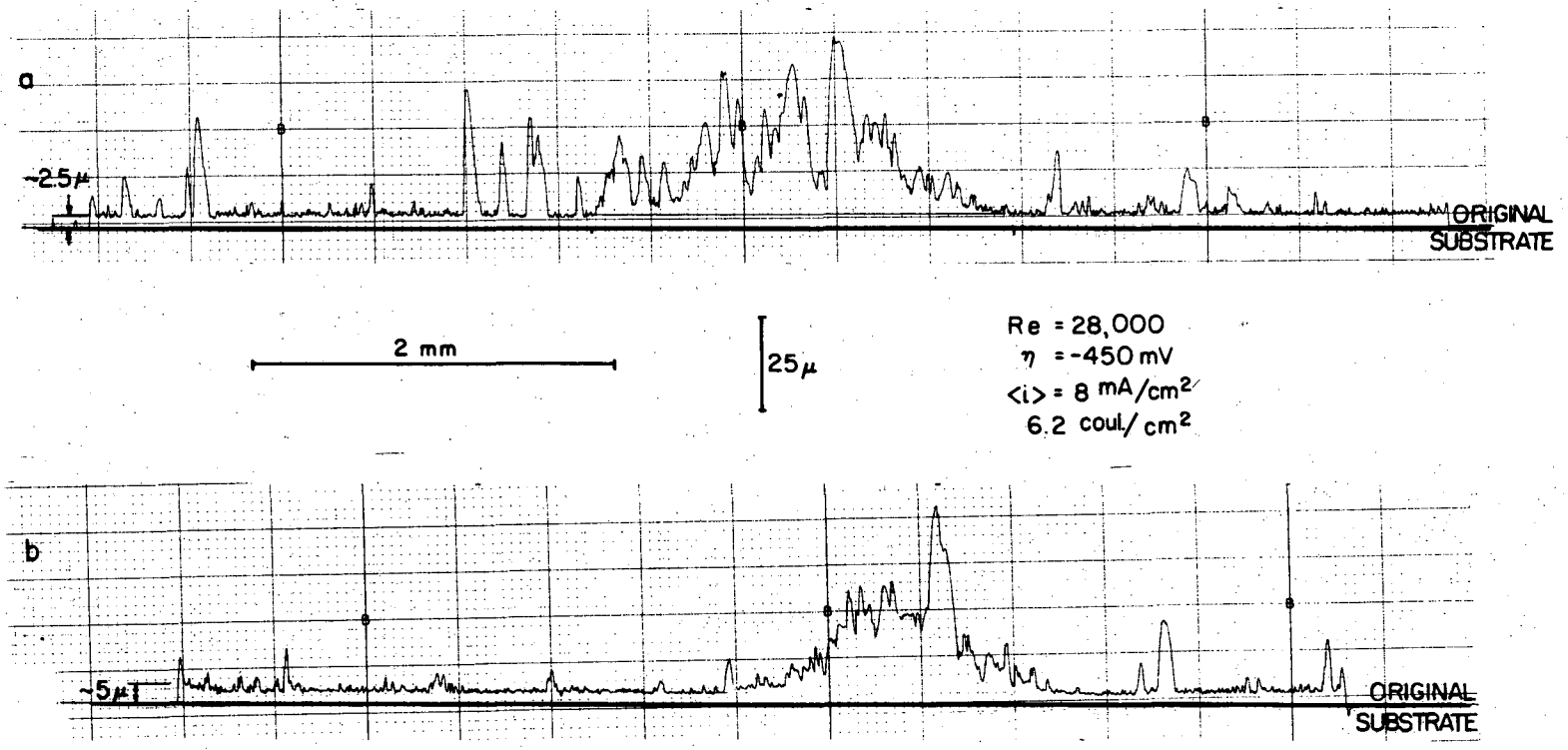

XBL 7410–1874

Fig. 16. Profiles made normal to the wake showing the absolute thickness of the deposit. The original substrate was made nonconducting in two strips parallel to the wake with acrylic.

of the porosity of the deposit. The profiles presented previously only showed relative changes in the deposit.

D. Quantitative Comparison of the Amount of Deposit Inside and Outside the Wake

The values of the amounts of deposit obtained are summarized in Table V along with the amount of deposit calculated from the current vs time curve. These measurements indicate the average current density in this portion of the far-wake is approximately twice that of the current density outside.

The ratio of the porosity inside to that outside the wake was estimated using the above values as representative of the weight of deposit per unit area and the surface profiles of Fig. 16 to calculate the ratio of the volumes.

$$\frac{\rho_w}{\rho_e} = \frac{W_w}{W_e} \cdot \frac{V_e}{V_w}$$

w = inside the wake
e = electrode surface outside the wake

The ratio (V_e/V_w) was determined from Figs 16a and 16b by comparing the area under the outline of the wake (the limits of the wake were defined as the beginning of the level deposit) using the substrate line as a reference to the area under a corresponding width of deposit with a thickness equal to that of the level region. The values of (V_e/V_w) obtained for a and b were 1/7.3 and 1/9.0. Taking 1/8 as a mean value for the volume ratio and 2 for the weight ratio (W_w/W_e)

$$\frac{\rho_w}{\rho_e} = 2 \cdot \frac{1}{8} = \frac{1}{4}$$

Table V. Quantitative comparison of deposit inside and outside the wake. (Re=27,900) Disc 3 inside wake.

Expt	Disc 1		Disc 2		Avg	Disc 3		Calc**	Ratio
	mg	mg/cm^2	mg	mg/cm^2	mg/cm^2	mg	mg/cm^2	mg/cm^2	$\frac{\text{Disc 3}}{\text{Avg}}$
1	3.38	3.55	3.65	3.83	3.69	0.36	7.35	3.63	1.99
2	6.05*	6.35	7.35	7.72	7.04	0.62	12.65	9.5	1.80

*Loss of deposit occurred during removal of disc at the end of the experiment.

**Calculated from I vs t curve for segment 7.

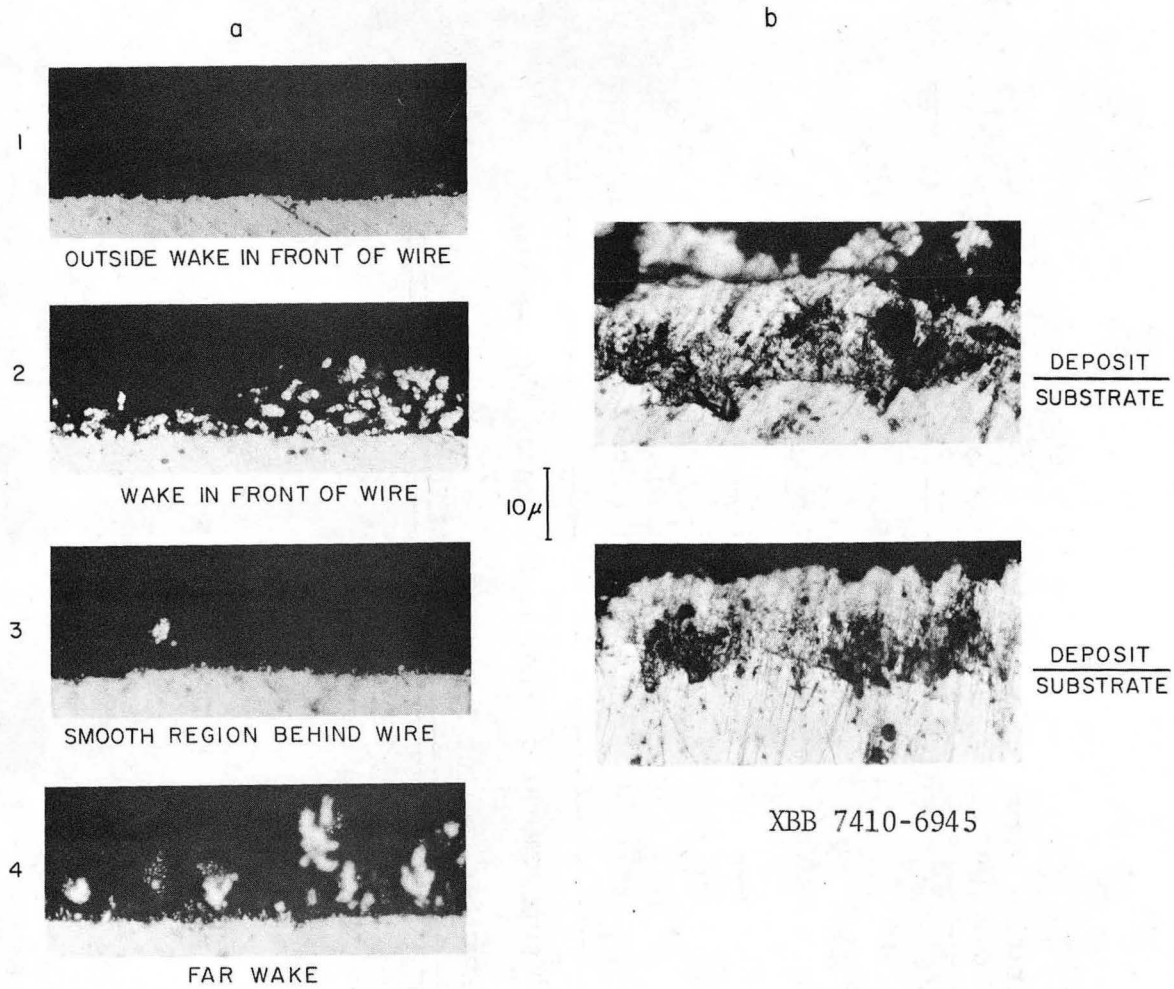

Fig. 17. a. Micrographs of the cross-sectioned electrode showing the powdery deposit in front of the wire and in the far wake. (Re=28,000, η=-480mV, $\langle i \rangle$=9.2 mA/cm^2, 6.2 coul/cm^2.)
b. Micrographs of a similar cross-section showing the boundary between the substrate and the powdery deposit. (Re=28,000, η=-450mV, $\langle i \rangle$= 10.8 mA/cm^2, 13.0 coul/cm^2).

E. Wake Cross-Section

The micrographs in Fig. 17 were obtained from the sectioned SEM electrodes using the Zeiss Ultraphot. The photos in Fig. 17a correspond to the following regions of the wake:

1. outside the wake in front of the cylinder
2. deposit in front of the cylinder
3. smooth region behind the cylinder
4. far wake

and Fig. 17b shows the boundary between the substrate and the porous copper of the deposit. The process of embedding the electrode in the Bakelite distorts the surface features, however the regions of powdery deposit remain distinguishable.

3.2. Surface Morphology

A. SEM Micrographs of the Deposit

The differences in porosity between the deposit inside and outside the wake are shown in Figs. 18c and 18d. The powder particle sizes in both regions (Figs. 18c and 18d) remains constant, ~1-3 μ. Inside the wake the particles grow in clusters with large volumes of interstitial space between these groupings as contrasted to the deposit outside the wake where on the average the particles are more uniformly distributed. (Micrograph c was not photographed at 10,000× because of the large void volume.) Clusters of particles or "dendrites" do appear outside the wake but they comprise a small percentage of the surface area. Figure 18a clearly shows the abrupt change in deposit morphology at the edge of the wake. (This is a view at the tip of one of the pincers.)

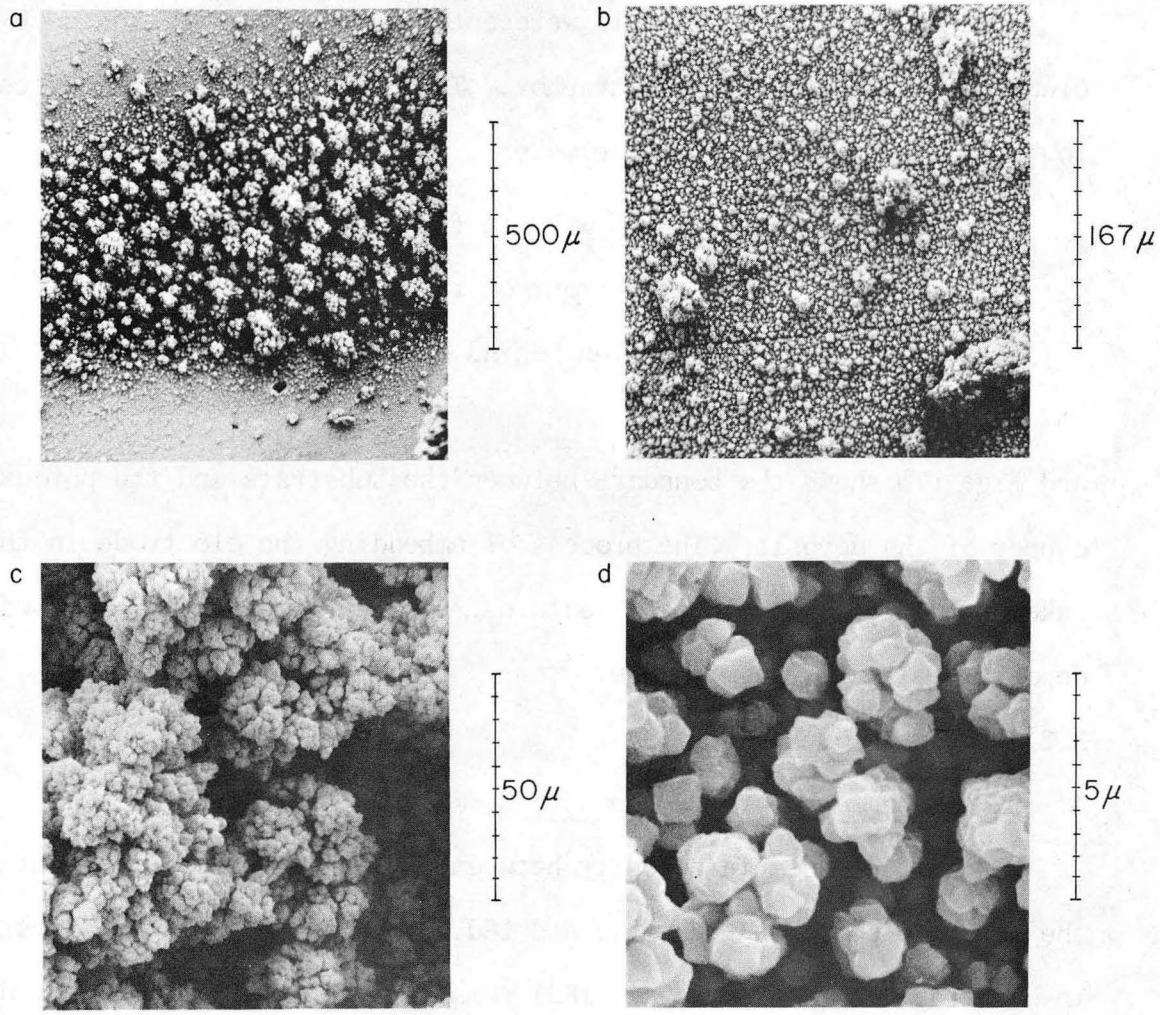

XBB 7410-6946

Fig. 18. Porosity of the deposit inside and outside the wake. (Re = 28,000, ⟨i⟩ = 10.8 mA/cm^2, ⟨coul/cm^2⟩ = 13.0, η = -350 mV).
a. Deposit in the tip of the tail.
b. Deposit outside the wake.
c. Deposit in the center of the far-wake.
d. Deposit outside the wake.

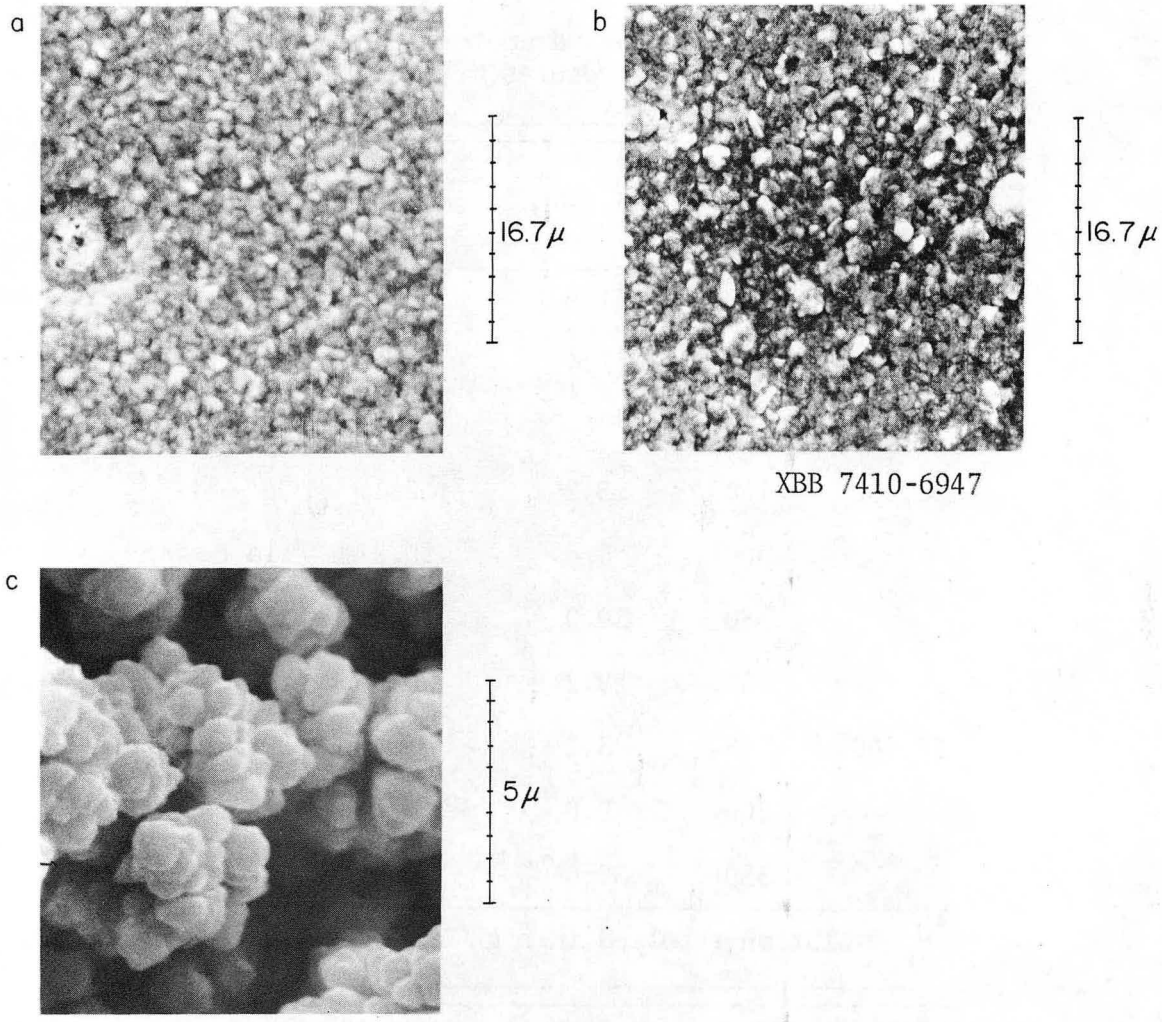

Fig. 19. a. Boulder type growth at η = -150 mV and Re = 3700.
b. Boulder type growth at η = -200 mV and Re = 3700.
c. Powdery type growth on a electrochemically polished surface at η = -350 mV.

Table VI. Experimental parameters for surface morphology results. (Figs. 19-22)

Re	n(-mV)	$\langle i \rangle \frac{mA}{cm^2}$	coul/cm^2	Figure
3,700	150	1.0	6.4	19a
	200	1.4	6.9	19b
28,000	150	5.2	12.4	20
	300	8.6	10.2	21a,b
	350	30.0	18.0*	18d
	400	9.2	6.2	21c,d
52,000	115	3.1	5.5	22a
	200	9.0	7.7	22b
	350	30.0*	18.0*	22c

*H_2 evolution resulted in high current densities.

B. The Effect of Overpotential and Substrate on the Deposit Morphology

The SEM micrographs in Figs. 19-22 show how the surface morphology changes with overpotential and substrate. The conditions under which each experiment was performed are listed in Table VI. For each flow rate (Re) the deposit was of an amorphous boulder type[7] at low overpotentials and developed into a powdery growth at the higher overpotentials. A comparison of the -115 and -150 mV (Figs. 19a, 20 and 22) and -200 mV (Figs. 19b and 22b) overpotential experiments at different flow rates shows that the type of deposit remains constant with increasing overpotential.

The mechanically and electrochemically polished surfaces produced radically different deposits at -150 mV as shown in Fig. 20. The mechanically polished surfaces have a more uniform boulder type roughness. The electropolished surface contained features of larger size with smooth continuous surfaces. To the eye the deposit on the electropolished surface appeared shiny. The mechanically polished surface appeared powdery with a dull finish. Contrary to what one would expect, surf-analysis profiles showed the deposit on the mechanically polished surfaces to have lower peak-to-recess dimensions. At -350 mV the deposit obtained on both types of substrate was of powdery nature as shown in Figs. 19c and 18d.

(Note: The dark area of Fig. 21a corresponds to an area which had been masked with acrylic. The large dendritic growth in the center was not typical of the deposit on the remainder of the electrode.)

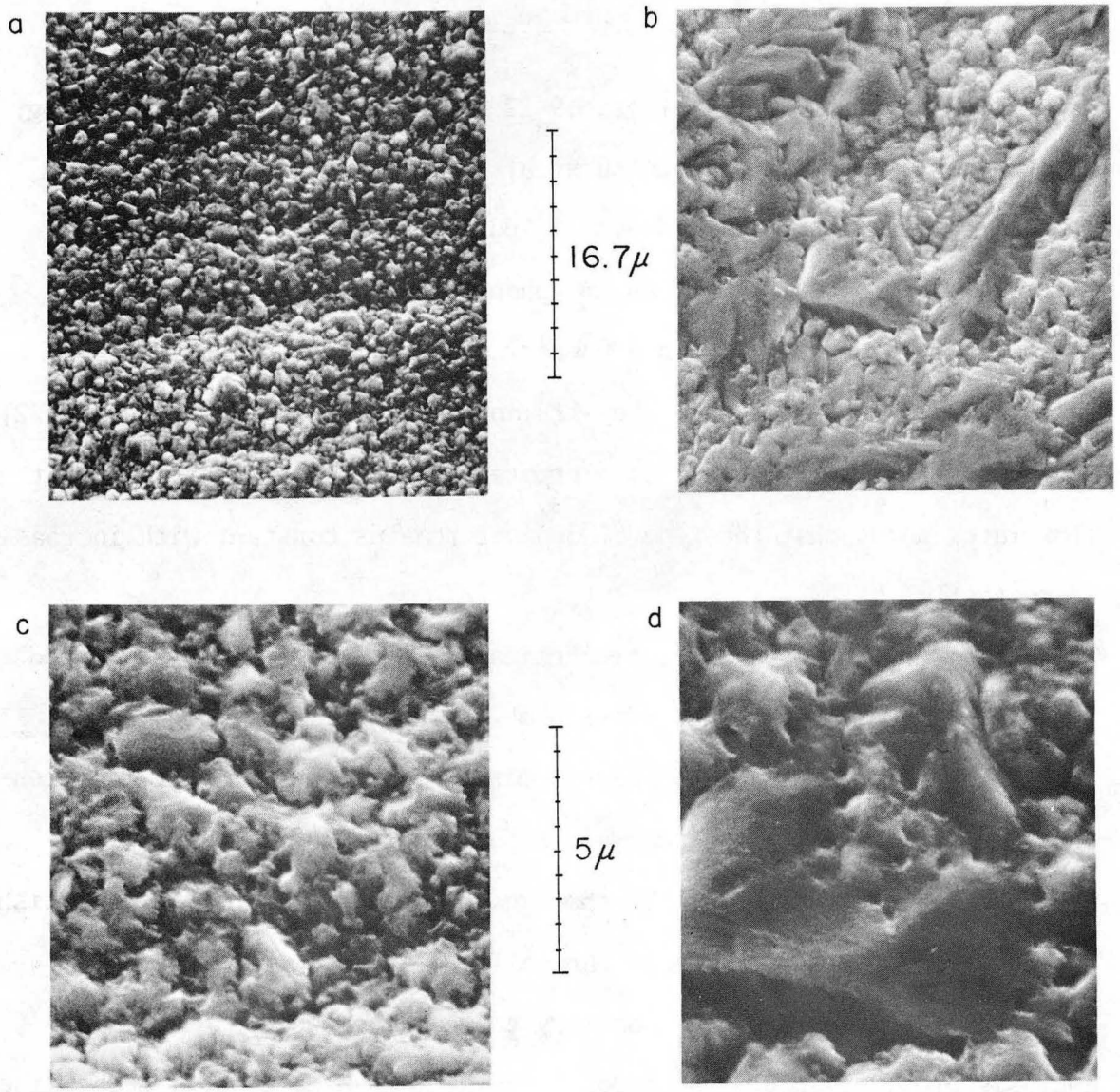

Fig. 20. Comparison of electrochemically and mechanically polished surfaces deposited on simultaneously. (η = -150 mV, Re = 28,000.)
a and c. Mechanically polished substrate.
b and d. Electrochemically polished substrate.
(c and d same deposit as a and b but with higher magnification.)

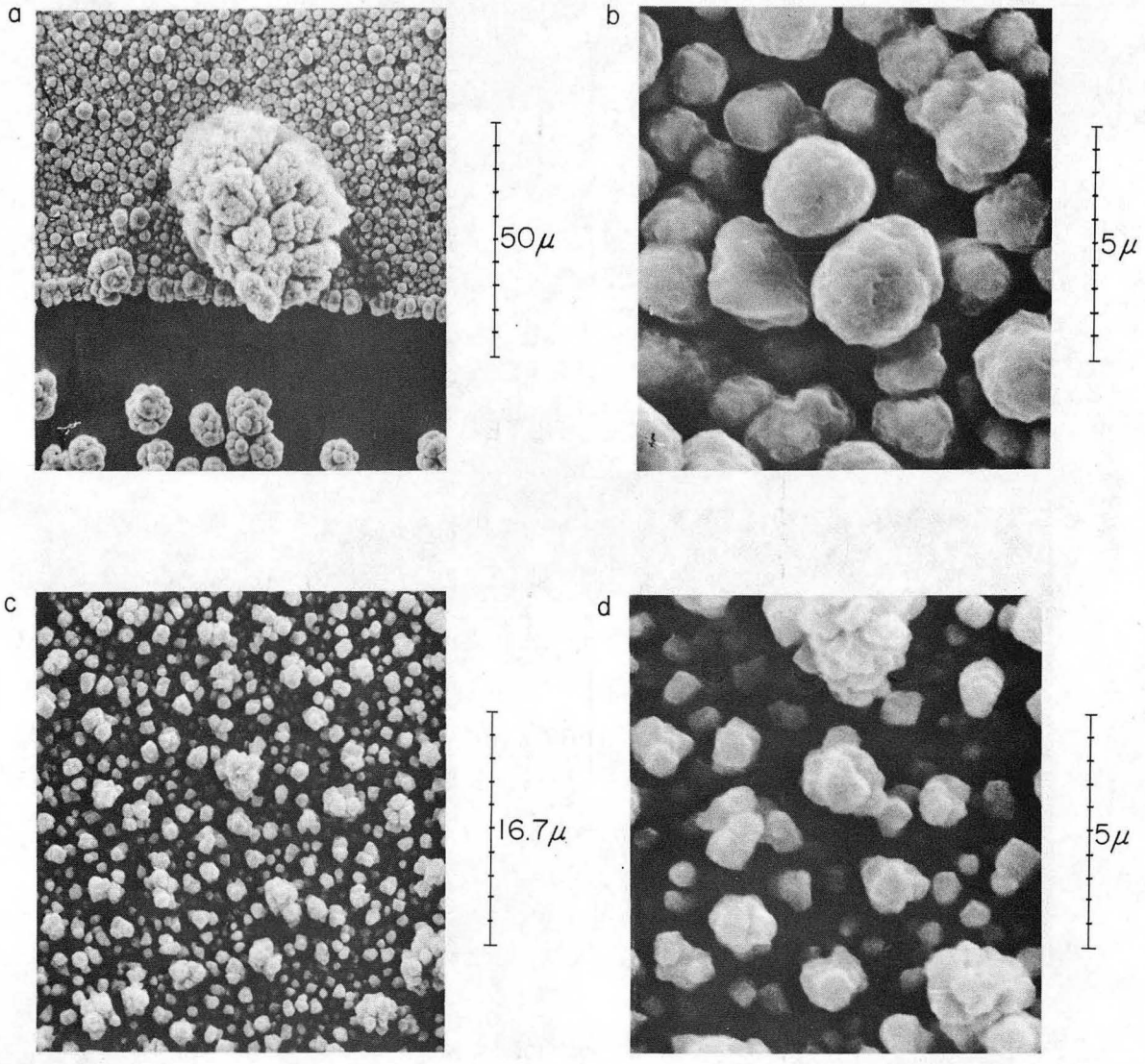

Fig. 21. Deposition at high overpotentials at Re = 28,000.
a and b. Powdery deposit at η = -300 mV.
c and d. Powdery deposit at η = -400 mV.

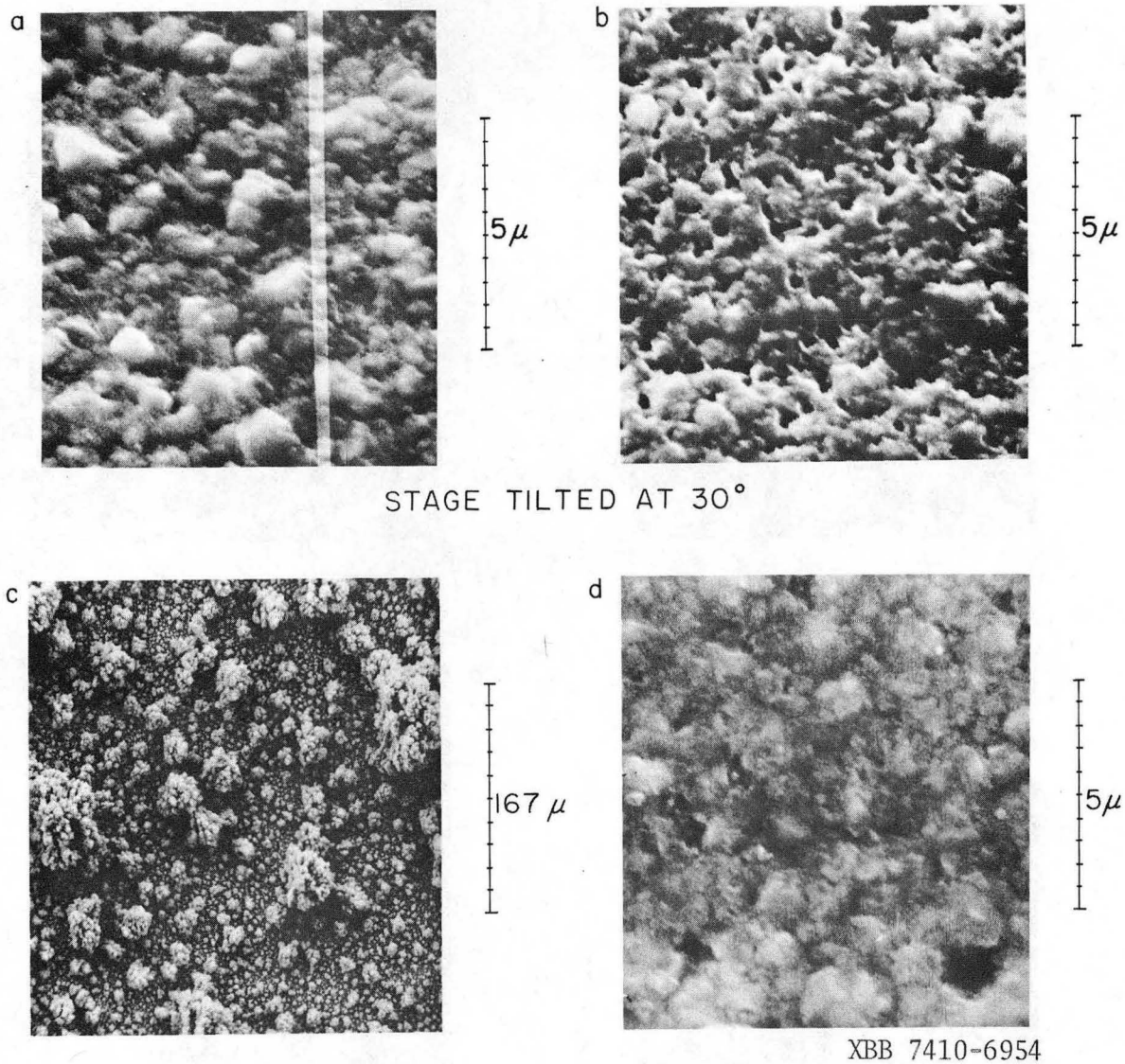

Fig. 22. Deposition at high Reynolds Number (Re = 52,000).
a. η = -115 mV
b. η = -200 mV
c. Electropolished substrate at η = -350 mV.
d. Micrograph of the same area shown in b with SEM stage at 0° inclination. This illustrates the necessity of inclining the stage for fairly "smooth" surfaces.

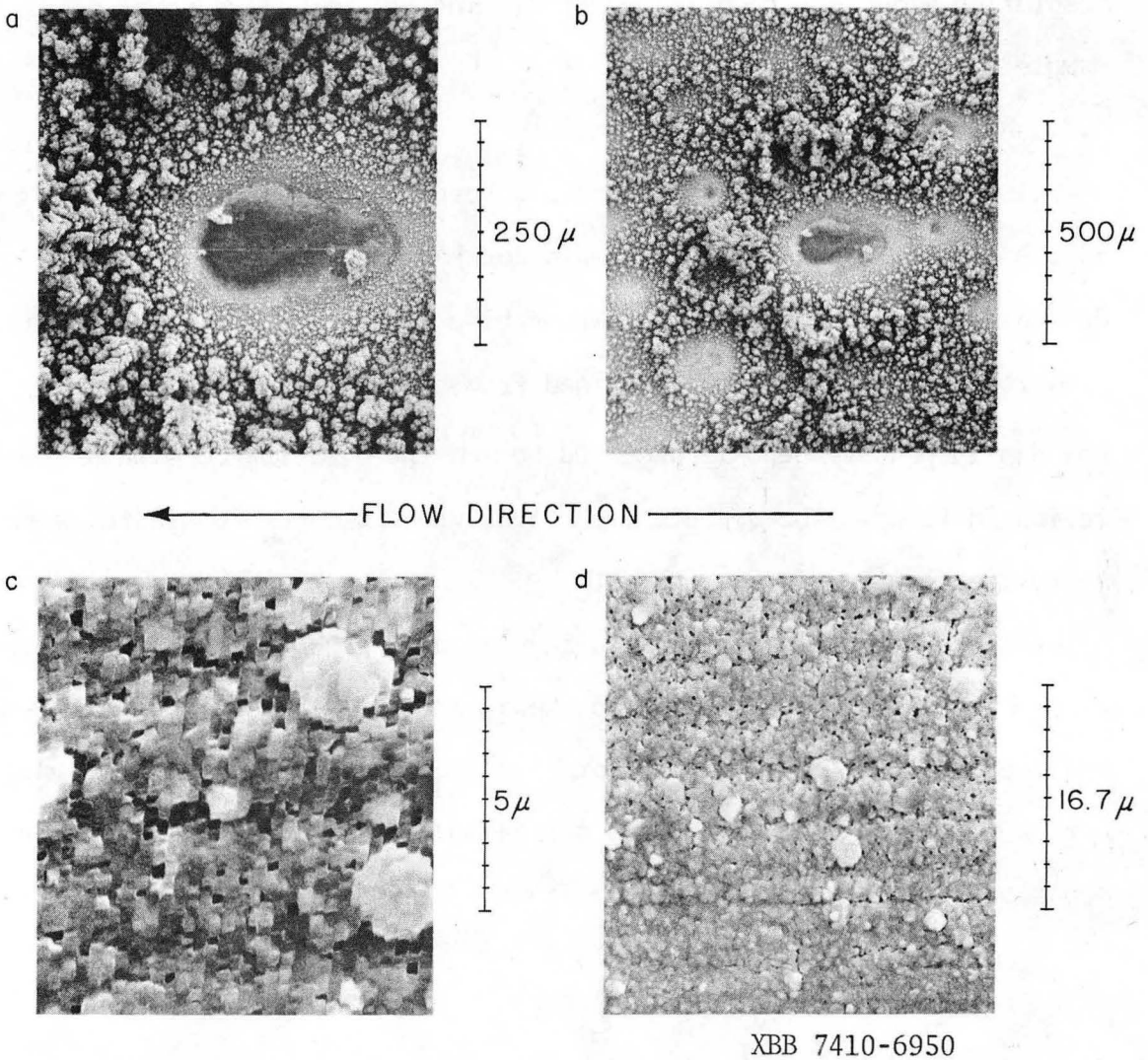

XBB 7410-6950

Fig. 23. a and b. Wake formation around air bubbles adhering to the electrode surface at low Reynolds number (Re = 13,000), η = -425 mV.

c and d. Orderly deposit obtained at η = -200 mV, $\langle i \rangle$ = 1.4 mA/cm^2, and t = 45 min. The parallel boundaries are normal to the direction of flow and the polishing striations. Micrograph c is a higher magnification view of d.

Figures 22b and 22d were included to show the improvement in resolution which can be obtained by tilting the SEM stage which holds the sample being observed.

3.3. Additional Results

In a number of experiments at low Reynolds number, (Re=13,000) bubbles adhered to the surface when the solution had not been completely deaerated. The wakes resulting from these bubbles (Figs. 23a and 23b) were opposite in nature to those obtained from the copper spheres. The buildup in powdery deposit occurred behind the disturbance with a "smooth" region in front. The deposit free areas where the bubbles rested were approximately 10 μ in diameter.

Figure 23c shows a deposit unique among those obtained in this series of experiments. The 0.25 μ strips were normal to the direction of flow and the polishing striations. Note the growths which appear to extend across the boundaries of several strips and the frequent breaks in the deposit. This experiment was run at Re = 13,000, n = -200 mV for 45 min.

IV. DISCUSSION

4.1. The Wake

The wake developes from local variations in the hydrodynamic, electrochemical, and mass transfer conditions induced by the presence of the protrusion. The effect of these variations are observed on two scales differing by three orders of magnitude: (1) On the macro-scale we see the overall shape of the wake (mm) and (2) on the microscale (microns) differences in the type of powder deposit appear. The discussion of the wake in the following paragraphs will follow the above organization.

A. The Macro-Scale

The secondary flow patterns caused by the presence of the protrusion initiate the chain of events which result in the formation of the wake. The outline of the wake delineated by the rough deposit shows us that these effects extend approximately 20 diameters downstream and 2 diameters upstream. The shape of the wakes in front of the wires and spheres agree with the flow patterns presented by White[6] in Fig. 1. As the flow impinges against the protrusion a roll cell develops around the base and separation of the boundary layer occurs. The wake perimeter indicates that this role cell extends past the protrusion forming the pincer like tails. The far-wake develops from the confluence of the eddies formed as the fluid flows off the trailing edge of the top of the protrusion and the roll cells formed around the base. (These details are not shown in Fig. 1.) Measurement of the amount of deposition shows these regions to be areas of more deposit (weight/unit area) than the rest of the electrode, consequently of higher agitation. The smooth region immediately

behind the protrusion and in between the tails must be a region of low agitation to be consistent with these results.

The top of the cylinder in Fig. 8 shows the effect of both the high current density at the edge and the turbulence caused by the flow impinging on the cylinder. The down-stream half of the top edge receives noticeably less deposit than the front. This may result from the separation of the boundary layer from the cylinder surface. The deposit around the entire perimeter of the edge is higher than the interior as a result of the increased current density there.

As the height of the cylinders in Figs. 6 and 7 decreased the extent of the wake did likewise until it almost disappeared at H = 0.1 mm. At a height of 0.1 cm the cylinder protrudes into the turbulent core causing the wake to develop. At a height of 0.01 cm the protrusion lies within the laminar sublayer. The values for the turbulent core and laminar sublayer are those given previously for Re = 30,000 (where the hydraulic diameter is the characteristic length), 0.01 cm and 0.06 cm. The Reynolds number for the cylinder of height 0.01 cm is approximately 10 (calculations are given in the Appendix). At this value of the Reynolds number the vortices behind the cylinder remain attached and the far-wake (or Ka'rma'm vortex-street) does not develop. The flow is in the transition region between laminar and turbulent flow. Goldstein[21] shows the effect of increasing the cylinder Reynolds number on vortex formation. For the 1.0 and 0.5 mm high cylinders downstream effects extended a minimum of 15 diameters. Around the protrusion, upstream and lateral changes in the deposit occurred within one or two diameters. The surface morphology of

the far wake gradually blends in with the rest of the electrode as the flow returns to a uniform state in contrast with clearly delineated boundary near the protrusion.

B. The Micro-Scale

a. Background. Any discussion of the wake should explain why a powdery deposit arises and continues to grow under these conditions. The picture is further complicated by the transient nature of the deposition surface. The relatively smooth, mechanically polished surface changes to a rough porous deposit as time progresses. Correspondingly, the microhydrodynamics near this surface undergoes a drastic transformation. As the height of the powdery deposit increases the mass transfer boundary layer is disturbed. The 3-dimensional character of the problem and turbulence of the flow permits only qualitative generalizations to be made of the interaction between surface and boundary

Ibl and co-workers[15,16,20] have developed a theory to explain the formation of powder deposits at the limiting current. A brief over-view of the main ideas will shed some light on the relevant parameters involved in the formation of the wake. First, most surfaces have some form of micro-roughness which for reasons of simplicity and analysis will be assumed to be in the form of a saw-tooth. The thickness of the mass transfer boundary layer above the roughness (δ_M) and the peak to recess height (h) are the important size parameters. The distribution of current on the roughness profile depends on the relative magnitudes of the resistance in the solution, the surface and concentration overpotentials and the ratio of δ_M/h.

The simplest case, the primary current distribution, occurs when overpotential is neglected and the resistance in the solution determines the distribution. Here peaks receive preferential deposition due to the lower resistance in the solution.

The secondary current distribution occurs when the surface overpotential determines the current distribution. Neglecting concentration overpotential a uniform current distribution will result if the resistance at the surface is greater than the resistance in the solution. This corresponds to an electrolyte with good "throwing power". When the concentration overpotential dominates ($i/i_L \rightarrow 1$), $\delta_M > h$, the current at the peaks will be higher than in the recesses due to the shorter diffusion length. The increased current density at the peaks tends to increase the surface overpotential there so the effect of the shorter diffusion path is reduced slightly. The above case occurs when the boundary layer is larger than the characteristic dimension of the roughness ($\delta_M > h$). When the boundary layer conforms to the roughness profile ($\delta_M < h$) surface overpotential again controls and a uniform current distribution results.

Additional geometric factors also tend to favor deposit at the peaks for $\delta_M > h$. The cross-section for mass transfer increases as the distance into the recess increases causing the flux to decrease. Peaks will also receive preferential deposition due to spherical diffusion.

Powder formation results from the high currents at the peaks. The mechanism of how the powder particle forms and what limits its size has not been clearly formulated to this authors knowledge. The role of mass transfer overpotential as described by Ibl was consistent with

the results of their experiments on the leveling action of addition agents at the limiting current.

b. Summary of the Results. (1) A thick powder deposit differentiated the wake from the rest of the electrode. On closer examination the deposit in the undisturbed region is also powdery in nature but of different structure (Fig. 18c and 18d). In experiments where dendritic* growth occurred outside the wake (such as in Fig. 8) a transition region of smooth deposit separated the wake from the rest of the electrode. In cases such as these, the amount of powdery deposit was much higher in the wake.

(2) Quantitative results show that the total current (I) per unit area inside the far-wake is approximately twice that outside. This test does not yield the true current density (i) because the area specified is the superfacial area not the surface area of the deposit. This will complicate the prediction of surface overpotential behavior which is expressed in terms of the true current density. The ratio of amount of deposit in the wake to that outside can be expected to increase around the protrusion where agitation is at its maximum.

(3) The increased amount of deposit in the wake indicates increased agitation or thinning of the boundary layer. This has been recently confirmed independently by Frank McLarnon in this laboratory using interferometric techniques to observe the boundary layer behind two-dimensional obstructions.

*The term dendritic is used loosely above since the features occurring here are clusters of powder particles not single crystals which have grown more rapidly when the surrounding deposit.

c. Discussion. The powdery nature of the deposit in-and outside the wake does not become evident until magnifications above 300× (Fig. 18b) are used. The appearance of powdery deposit (in both regions) should not be surprising since deposition occurred at the limiting current. The differences arise in the "fine" structure of the deposit as shown in Figs. 18c and 18d. The deposit in the wake occurs in dense clusters of powder particles with large interstitial volume between them ($\rho_w/\rho_e \sim 1/4$). Outside the wake the powder particles are more uniformly distributed with growth taking place in a vertical direction. (In some places the powder particles grow on top of one another to form columns.) The large outgrowths (or "dendrites") in the "smooth" region resemble the powder clusters in the wake.

For the experiments presented here the mass transfer boundary layer assuming a flat surface varied from 15 μ at Re = 28,000 to 9 μ at Re = 52,000. The surface after polishing has roughness elements of $h < 1$ μ. The powder particles were 2-5 μ and the height of the deposit in the wake above that outside varied from 25-50 μ. Initially δ_M/h is approximately 1 in the wake and 3 outside the wake for the powder particles at Re = 28,000. As soon as dendritic growth occurs in the wake the above value will decrease. These numbers provide some idea of the dimensions involved in the following discussion.

The large outgrowths (or "dendrites") in the "smooth" region resemble the powder clusters in the wake.

The differences can be explained using the concepts presented by Ibl. Initially the solution sees the same substrate with differences existing only in the solution. In the wake region the boundary layer has thinned to approximately 50% of that outside and the total current (I) and current density (i) have increased proportionately. The structure of the deposits indicate that two regimes exist:

(1) inside the wake $\delta_M < h$

(2) outside the wake $\delta_M > h$.

In case (2), assuming a uniform roughness, the peaks initially act as growth sites for powder formation. As the deposit grows δ remains constant and the peaks (now powder particles) remain preferred for deposition continuing the vertical growth.

In contrast the reduced boundary layer in the wake initially causes rapid growth of any surface imperfections. As these features disturb the mass transfer boundary layer, δ_M decreases to the order of h and deposition occurs over the entire profile. This three-dimensional growth results in the formation of the powder clusters. The large interstitial volume arises as the isolated growth sites increase in height occluding the areas in between from the flow. These stagnant regions are now inaccessible to current. (This process occurs outside the wake at a slower rate where large dendritic powder clusters can be seen forming.) Once the surface has been roughened in this manner the process is self-propagating.

Due to the roughness of the deposit in the wake, the fluctuating nature of highly turbulent flow, and the transient nature of the surface the quantities δ and h are not well defined. It is assumed in the above analysis that "δ_M" and "h" remain constant with time. However, as the experiment proceeds the surface roughens and both these values change. In the wake the increased roughness causes the surface to disturb the boundary layer to a larger extent. In the region outside the wake δ_M must remain larger than h for the vertically orientated growth to continue since the peaks must be in a favorable position for mass transfer. As shown in Fig. 18b this requirement will not be satisfied after long times due to the increased "dendritic" growth.

The preceeding analysis only considers the effect of mass transfer because at the limiting current surface overpotential and the iR drop in the solution are negligible compared to the concentration overpotential. Initially, the increased current density may cause an increase in the surface overpotential which can result in hydrogen evolution assuming i/i_L remains constant (equal to that outside the wake). Ibl[16] has shown that hydrogen evolution does not cause powder formation but the generation of bubbles will effect the stirring and current distribution at the surface. This does not require alteration of the overall analysis presented above.

The transition region between the wake and undisturbed deposit and the smooth region behind the protrusion remain to be explained. The outside perimeter of the wake corresponds to the separation line shown in Whites schematic (Fig. 1). Outside this boundary the agitation decreases in magnitude finally reaching that of the undisturbed region.

The wake, due to the thinner boundary layer, acts as a current collector causing a decrease in current in regions immediately adjacent to it. This decrease results in deposition below the limiting current here. As observed earlier reducing i/i_L to 0.9 has a pronounced smoothing effect. Behind the protrusion a stagnant region developes and deposition again occurs below the limiting current resulting in the smooth deposit.

In summary the deposit morphology in the wake forms as a result of: (1) the increased amount of deposit per unit of superfacial area caused by the thinner boundary layer and (2) the three-dimensional growth of the surface roughness elements.

C. Wakes Around Gas Bubbles

The wakes formed around gas bubbles attached to the surface, differ in appearance from those obtained in the experiments with copper spheres. In making a comparison of the two cases the following differences must be allowed for:

(1) Bubble diameters equal approximately 0.1 mm vs 0.65 mm for the copper spheres.

(2) The bubbles deform into a oblong shape with the major axis in the direction of the flow.

(3) In some instances the bubbles are densely packed as contrasted to the isolated spheres.

As noted previously, the tendency for the boundary layer to form a roll cell decreases as the height of the protrusion decreases. This may explain the lack of rough deposit in front of the bubble wakes. As the bubbles are deformed the rear will increase in height resulting in a shape similar to a inclined plane. The boundary layer may separate

at this rear edge causing the wake to form behind the bubble as seen in Figs. 19a and 19b.

4.2. Surface Morphology

Observation of the surface morphology on flat surfaces was made concurrently with those of the wake. As expected the deposit changed from compact to powdery as the overpotential increased. The role surface and mass transfer overpotential play in determining the surface morphology is clearly shown in the comparison of deposition on mechanically and electropolished surfaces. At low overpotential, where surface overpotential dominates, the deposit obtained changed noticeably with the type of substrate (Fig. 20). At higher overpotentials, η = -350 mV, diffusion is controlling and powdery deposit is obtained on both types of surface (Figs. 21 and 22c). The differences in the powdery deposit in these figures arise from the higher flow rate used in Fig. 22.

The orderly deposit shown in Fig. 23 is considered anomalous. After this experiment the solution was changed for other work preventing duplication of the conditions.

The results of these experiments provide a reference to compare the morphology of the wake to. Literature reports of surface morphology cannot be relied upon because of the unavoidable differences in solution properties, especially when working with a large system (80 gal of electrolyte) as in these experiments.

V. FUTURE WORK

The foregoing qualitative description derived from SEM micrographs, macro-photographs, and surface profiles shows how in the cathodic deposition of copper the wake varies around cylindrical and spherical protrusions as a function of height, diameter, and the interrelated parameters of overpotential, current density and flowrate. The height of the protrusion and the overpotential, i/i_L, are the critical parameters which determine whether a wake will appear.

The reduced boundary layer thickness and increased current density arising from the turbulence induced by the protrusion results in the formation of the wake. This analysis, based only on mass transfer considerations using the available data, explains the results in the simplest manner possible.

Further study of the wake should include:

(1) Accurate determination of the current density distribution around the protrusion by a sectioned electrode. Formation of the porous deposit in the $CuSO_4$ system dictates that a redox system such as $Fe(CN)_6^{3-}$ -- $Fe(CN)_6^{4-}$ (Ferri-Ferro cyanide system) be used to prevent shorting of the segments.

(2) Experiments of the kind described in (1) will indicate variations in the turbulence intensity on the surface. Verification of these measurements by visualization of the flow above the electrode surface will add to the understanding of why the wake assumes the shape it has.

(3) Observation of deposition on isolated roughness elements ($h = 5$ microns) as a function of the boundary layer thickness will

confirm or disprove the hypothesises proposed above concerning 3-dimensional growth.

(4) Experiments of shorter duration to determine when the morphology of the deposit inside and out the wake begin to differ.

NOMENCLATURE

c	concentration (moles/liter)
I	total current
i	current density (current/unit area)
i_L	limiting current density
Sc	Schmidt number (ν/D), dimensionless
h	height of protrusion
ρ	density of solution (g/ml)
$\rho_{(\ )}$	weight copper per unit volume
δ_M	mass transfer boundary layer thickness
D	diffusivity (cm^2/sec)
ν	kinematic viscosity (cm^2/sec)

ACKNOWLEDGEMENTS

I would like to express my deep appreciation and gratitude to Professor Charles Tobias for his direction and support throughout this work. Professors R. Muller and L. Talbot are gratefully acknowledged for their review of this manuscript.

I would also like to thank Mr. Uziel Landau for his assistance and advice, to Mr. R. White and Mr. J. Trainham for proof reading the manuscript and to Miss Jean Wolslegel for typing this thesis.

This work was done under the auspices of the U. S. Atomic Energy Commission.

APPENDIX

1. Mass transfer boundary layer thickness from limiting currents.

   A. Assumptions:

      a) Large excess of supporting electrolyte (H_2SO_4) reduces transference number of Cu^{++} to zero.

   B. Fick's Law then reduces to the following equation at the limiting current.

$$i_L = \frac{DnF}{\delta} C_b$$

   C_b = bulk conclusion of Cu^{++}

   δ = equivalent film thickness

   n = equivalents/mole

   D = diffusivity

   i_L = limiting current

   C. Sample calculation.

   Solution B

$$C_b = 0.021 \text{ M}, \; n = 2, \; D = 3.8 \times 10^{-6} \text{ cm}^2/\text{sec}$$

$$\text{let } i_L \approx 0.01 \text{ A/cm}^2$$

$$\text{then } \delta = 16 \; \mu$$

2. Location of laminar sublayer and turbulent core.

The hydrodynamic boundary layer is fully developed at the beginning of the electrode. The correlation of R. G. Deissler (Fig. 5.3-1)[22] given by Bird, Stewart and Lightfoot will be used to estimate the laminar sublayer and turbulent core. The correlation which was obtained for smooth pipes can be applied to rectangular cross-sections if the hydraulic diameter is used. (The hydraulic diameter as defined in Bird[22] is one-half that used in this report.)

$$S^+ = sv_*\rho/\mu$$

$$v_* = (\tau_o/\rho)^{1/2} = \langle v_z \rangle (f/2)^{1/2}$$

s = distance from wall

S^+ = dimensionless distance from wall

τ_o = shear stress at wall

f = friction factor

The Blasius formula for f applies for the range of Reynolds number used here.

$$f = \frac{0.0791}{Re^{1/4}}$$

For a Reynolds number of 30,000 (15,000 as defined in Ref. 22)

$$f = 0.007 \text{ and } v_* = 7.8 \text{ cm/sec}$$

The physical properties of solution B will be used

$$\nu = (\mu/\rho) = 0.018 \text{ cm}^2/\text{sec}$$

Laminar Sublayer $\quad 0 \leqslant S^+ \leqslant 5$

$$S = \frac{(0.018)(5)}{7.8} = 0.0115 \text{ cm} \approx 0.1 \text{ mm}$$

Turbulent Core $\quad S^+ \geqslant 26$

$$S = \frac{(0.018)\ 26}{7.8} = 0.0599 \text{ cm} \approx 0.6 \text{ mm}$$

3. Reynolds number of the 0.1 mm high cylinder.

$$Re_c = \frac{\langle v_c \rangle h}{\nu}$$

h = height of cylinder

$\langle v_c \rangle$ = average velocity over the height of the cylinder

$s = 0.1$ mm $\qquad S^+ = 4.31$

The cylinder lies within the laminar sublayer and the velocity reduces to

$$v^+ = S^+ \qquad \text{where } v^+ = \frac{\bar{v}_z}{v_*}$$

$$\langle v_c^+ \rangle = \frac{y^+}{2} = \frac{4.31}{2} = 2.15$$

$$\langle v_c \rangle = 7.8 \times 2.15 \cong 17 \text{ cm/sec}$$

$$Re_c = \frac{\langle v_c \rangle h}{\nu} = \frac{17(0.01)}{0.018} \approx 10$$

$Re_c \approx 10$ at a channel Reynolds number of 30,000.

REFERENCES

1. T. K. Ross and R. K. Badhawar, Corrosion Science 5, 29 (1965).
2. D. A. Dawson and Olev Trass, Int. J. Heat Mass Trans. 15, 1317 (1972).
3. U. Landau, Ph. D. Thesis, LBL-2702, in progress.
4. Inorganic Materials Research Division Annual Report 1973, Lawrence Berkeley Laboratory, University of California, Berkeley.
5. V. G. Levich, Physicochemical Hydrodynamics (Prentice-Hall, Inc., N. J., 1962), p. 162.
6. F. M. White, Viscous Fluid Flow (McGraw Hill, N. Y., 1974), p. 365.
7. J. P. Johnston, J. Basic Eng., 233 (1960).
8. R. D. Naybour, Electrochimica Acta 13, 763 (1968).
9. I. N. Justinijanovic' and A. R. Despic', Electrochimica Acta 18, 709 (1973).
10. J. O'M. Bockris, Z. Nagy and D. Drazic, J. Electrochem. Soc. 120 30 (1973).
11. H. Y. Cheh and R. Sard, J. Electrochem. Soc. 118, 1737 (1971).
12. H. J. Pick, G. G. Storey and T. B. Vaughn, Electrochimica Acta 2, 165 (1960).
13. T. B. Vaughn and H. J. Pick, Electrochimica Acta 2, 179 (1960).
14. S. C. Barnes, G. G. Storey and H. J. Pick, Electrochemica Acta 2, 195 (1960).
15. N. Ibl and K. Schadegg, J. Electrochem. Soc. 114, 54 (1967).
16. N. Ibl, Ph. Javet and F. Stahel, Electrochimica Acta 17, 733 (1972).
17. N. Ibl, G. Gut and M. Weber, Electrochimica Acta 18, 307 (1973).

18. I. Baker and R. S. Gibbs, Ind. and Eng. Chem. 18, 124 (1946).

19. J. W. Diggle, A. R. Despic and J. O'M. Bockris, J. Electrochem. Soc. 116, 1503 (1969).

20. N. Ibl, Diffusion Layers; Influence of Mass Transport on the Structure of Electrolytic Deposits, Proceedings of ⟨⟨Surface 66⟩⟩, p. 48.

21. S. Goldstein, Modern Developments in Fluid Dynamics (Oxford University Press, 1938), p. 62.

22. R. B. Bird, W. E. Stewart and E. N. Lightfoot, Transport Phenomena (Wiley and Sons, Inc., 1960), p. 163.

TECHNICAL INFORMATION DIVISION
LAWRENCE BERKELEY LABORATORY
UNIVERSITY OF CALIFORNIA
BERKELEY, CALIFORNIA 94720